Biogeosciences Discuss., doi:10.5194/bg-2016-153, 2016
Manuscript under review for journal Biogeosciences
Published: 30 May 2016

Biogeosciences Discussions Open Access EGU

Physical control of the interannual variations of the winter chlorophyll bloom in the northern Arabian Sea

M.G. Keerthi[1], Matthieu Lengaigne[2, 3], Marina Levy[2], Jerome Vialard[2], V. Parvathi[1], Clément de Boyer Montégut[4], Christian Ethé[2], Olivier Aumont[2], I. Suresh[1], P.M. Muraleedharan[1]

[1] CSIR-National Institute of Oceanography (CSIR-NIO), Goa, India

[2] Sorbonne Universités (UPMC, Univ Paris 06)-CNRS-IRD-MNHN, LOCEAN Laboratory, IPSL, Paris, France

[3] Indo-French Cell for Water Sciences, IISc-NIO-IITM–IRD Joint International Laboratory, NIO, Goa, India

[4]Laboratoire d'Océanographie Spatiale, IFREMER, Brest, France

Correspondence to: M.G. Keerthi (keerthanaamg@gmail.com)

Abstract. The northern Arabian Sea hosts a winter chlorophyll bloom, triggered by convective overturning in response to cold and dry northeasterly monsoon winds. There is currently no consensus about the processes responsible for the interannual variations of the magnitude of this bloom. The current study aims at identifying these processes using both observations (including remotely sensed chlorophyll data and physical parameters derived from Argo data) and a coupled biophysical ocean model simulation. Six different remotely sensed chlorophyll products are compared and they show a good phase agreement at seasonal and interannual timescales, but significant discrepancies in bloom amplitude. Both model and observations indicate that the interannual fluctuations of the winter bloom amplitude are strongly tied to mixed layer depth interannual anomalies (correlation ~0.6 to 0.7), which are themselves controlled by the net heat flux at the air-sea interface. Our results suggest that mixed layer depth control of the bloom amplitude ensues from the modulation of nutrient entrainment into the mixed layer. In contrast, our results show insignificant correlations between the bloom amplitude and thermocline depth, which precludes a control of the bloom amplitude by daily dilution down to the thermocline depth, as suggested in a previous study.

Biogeosciences Discuss., doi:10.5194/bg-2016-153, 2016
Manuscript under review for journal Biogeosciences
Published: 30 May 2016

1 Introduction

Located in the western arm of the northern Indian Ocean, the Arabian Sea (AS) is forced by energetic seasonally reversing monsoon winds, which largely control its physical properties. During boreal summer, strong southwesterly winds blow over the western AS (Findlater, 1969) and cause intense upwelling along the coasts of Somalia and Oman and downwelling in the central AS (e.g. Schott and McCreary, 2001). During boreal winter, the Eurasian continent cools and a high-pressure region develops on the Tibetan plateau, resulting in cold and dry north/northeasterly winds (e.g. Smith and Madhupratap, 2005) and leading to strong evaporative cooling (Dickey et al., 1998). These diverse physical processes cause substantial variations in marine biogeochemical and ecosystem response. Being one of the most productive regions in the world ocean (Satyaprakash et al., 2007; Prasanna Kumar et al., 2000) and being home to the second most intense oxygen minimum zone in the world ocean (Kamykowski and Zentara, 1990), the AS provides an excellent test bed for studying biophysical coupled processes (McCreary et al., 2009).

Previous studies have extensively described the seasonal variability of surface chlorophyll in the AS. The AS biogeochemical properties vary from stratified oligotrophic conditions during inter-monsoon periods to eutrophic conditions during monsoons (Smith et al., 1998; McCreary et al., 2009). Neither surface irradiance nor temperature limits the biological productivity in this tropical basin: instead, it is mostly attributed to dynamical processes in response to the monsoonal forcing (e.g. Barber et al., 2001; Marra and Barber, 2005). During boreal summer, the largest seasonal blooms are found along the coasts of the Arabian peninsula (e.g. Banzon et al., 2004; Lévy et al., 2007; Wiggert et al., 2005) and are exported offshore by mesoscale eddy stirring (e.g. Resplandy et al., 2011). In boreal winter, convective overturning allows entrainment of nutrients into the mixed layer and leads to a prominent bloom in the northern AS (Banse and English, 2000; Madhupratab et al., 1996; Prasanna Kumar et al., 2001; Wiggert et al., 2002). In addition to these seasonal variations, several studies revealed large interannual variations in the AS winter chlorophyll from either satellite (Banse and McClain, 1986; Banse and English, 1993; Sarma et al., 2006; Wiggert et al., 2002; Sarma et al., 2012) or in-situ measurements (Bauer et al., 1991; Madhupratap et al., 1996; Gundersen et al., 1998; Prasanna Kumar et al., 2001). This strong interannual variability of the northern AS winter bloom is illustrated on Fig. 1a-b for two consecutive winters. A particularly intense bloom developed in the northern AS during winter 2008 (Fig. 1b), with high surface chlorophyll concentration (>1.0 $mg.m^{-3}$) extending southward down to 14°N. In contrast, the winter 2007 bloom remained confined to the northern AS (Fig. 1a), with high chlorophyll concentration (>1.0 $mg.m^{-3}$) limited to the north of 20°N. The difference in the amplitude of the bloom between winter 2007 and 2008 averaged over the northern AS box (hereafter NAS region shown in Fig. 1) reaches 0.23 $mg.m^{-3}$, which is approximately 30% of the climatological winter chlorophyll value.

Understanding the mechanisms driving these chlorophyll interannual variations is important, as this might have a profound influence on the variations of the fish stocks and of the oxygen minimum zone in the AS. To date, only a few studies have

Biogeosciences Discuss., doi:10.5194/bg-2016-153, 2016
Manuscript under review for journal Biogeosciences
Published: 30 May 2016

discussed the mechanisms that could be responsible for the winter bloom interannual fluctuations (Banse and McClain, 1986; Prasanna Kumar et al., 2001; Wiggert et al., 2002) and no consensus has been reached so far. Comparing in-situ time series in February 1995 and 1997, Prasanna Kumar et al. (2001) suggested that increased convective cooling resulted in an intense convective mixing, a deeper mixed layer depth (hereafter, MLD), enhanced nutrients injection through entrainment and ultimately a stronger bloom in winter 1997 than in winter 1995. Keerthi et al. (2015) confirmed that large MLD variations occur in winter in the NAS, which are largely driven by fluctuations in the advection of dry, cold air from the continent, but did not investigate their biogeochemical consequences. Comparing three consecutive winters from 1998 to 2000, Wiggert et al. (2002) suggested, using a simple one-dimensional model, that interannual variations of the bloom intensity were not controlled by interannual MLD variations, but rather by the night-time penetration of diurnal mixing, whose downward penetration is regulated by the thermocline depth (hereafter, TCD). In this paradigm, a deeper TCD allows for a deeper night-time mixing, a greater dilution of phytoplankton biomass and stronger inhibition of the bloom development. However, it should be noted that these previous studies based their conclusions on the analysis of a very limited number of winters.

In the present paper, we aim at describing and better understanding the interannual variability of the NAS winter bloom. On the observational side, this study benefits from the increased temporal coverage of the satellite chlorophyll data (~15 years) and the advent of the ARGO program that allows monitoring in-situ MLD and TCD variations from 2002 onwards, which allows us to perform a direct comparison between these physical parameters and the chlorophyll variability. In addition to these satellite and in-situ observations, we analyse outputs from a coupled biophysical model simulation. The analysis of this simulation, which accurately simulates NAS winter chlorophyll interannual variations, allows us to investigate the subsurface processes not readily available from observations. Section 2 describes the observational products (satellite chlorophyll estimates and ARGO-derived MLD and TCD; Section 2.1) and the numerical experiment (Section 2.2). Section 3 provides an intercomparison of the available satellite chlorophyll products (Section 3.1) and the model evaluation (Section 3.2). Section 4 provides a description of the chlorophyll interannual variability, its relationship with physical parameters and discusses the mechanisms driving these fluctuations. Section 5 finally provides a summary and discussion of our results.

2 Data and Method

2.1 Observations

The surface chlorophyll (hereafter, SChl) estimates analyzed in the present study are derived from different instruments (SeaWiFS, MERIS and MODIS), retrieval algorithms and span different periods (Table 1). We used the Level-3 Standard Mapped Images with a 9x9-km spatial and a monthly temporal resolution downloaded from http://oceancolor.gsfc.nasa.gov for all of these single-mission products. In addition, we also used three level 3 merged ocean-color products downloaded

Biogeosciences Discuss., doi:10.5194/bg-2016-153, 2016
Manuscript under review for journal Biogeosciences
Published: 30 May 2016

from http://www.oceancolour.org/ at 4x4-km and monthly resolution: The weighted average empirical (AVW) product, the semi-analytical Garver Siegel Maritorena (GSM) product and the OC-CCI product from the Ocean Color Climate Change Initiative (OC-CCI) product. The longest observational period is provided by the OC-CCI product and spans from October 1997 to December 2013.

The ocean physical parameters are derived from an updated version of the dataset described in Keerthi et al. (2013), which now has a temporal coverage extended to 2013 and includes an estimate of the TCD in addition to the MLD. This dataset is built from a combination of Argo and historical temperature and salinity profiles. MLDs were estimated using a temperature criterion, and are defined as the depth where the temperature increases by 0.2°C with respect to the temperature at 10 m. The reference depth was taken at 10 m to avoid aliasing by the diurnal cycle. The TCD was defined as the depth of the maximal vertical temperature gradient. MLDs and TCDs were estimated from individual temperature profiles at their native vertical resolution. The resolution of the data was then degraded to a regular 2^o monthly grid, by taking the median of all MLDs and TCDs in each grid mesh. A more detailed description of this procedure can be found in Keerthi et al. (2013). An overview of the spatio-temporal coverage of this dataset over the NAS is provided in Fig. 2. While the data coverage is particularly sparse in winter before 2002 in our targeted region (e.g. less than 10 data per month are available in winter 2000 in the NAS region), the data density considerably increased after 2002, with the development of the Argo program in that basin (Fig. 2a). After 2002, the winter data density ranged from 25 data per month during 2005 to nearly 120 data per month during 2012. Note that the data coverage is also spatially inhomogeneous, with the highest coverage along a shipping line crossing the NAS box (Fig. 2b).

We also use the World Ocean Atlas (WOA13) climatology (Boyer et al., 2013) to derive climatologies of the thermocline and nitracline depths, calculated as the depths of maximum temperature and nitrate gradients, respectively. Wind speeds, surface air temperatures and net heat fluxes are derived from the Tropflux product (Praveen Kumar et al., 2012).

2.2 Model configuration and numerical experiments

These observational products are complemented by a biophysical model simulation, which allows extending our analysis over a longer time period and analysing depth-integrated biogeochemical properties not captured by satellites. We use the NEMO (Nucleus for European Modelling of the Ocean; see Madec (2008) for an exhaustive description) ocean general circulation model coupled with the PISCES (Pelagic Interaction Scheme for Carbon and Ecosystem Studies; see Aumont et al. (2015) for an exhaustive description of the model) biogeochemical component. PISCES has 24 compartments, which include two sizes of sinking particles and four "living" biological pools, that represent two phytoplankton (nano-phytoplankton and diatoms) and two zooplankton (micro-zooplankton and meso-zooplankton) size classes. Phytoplankton growth is limited by five nutrients: NO3, NH4, PO4, SiO4, and Fe. The ratios among C, N, and P are kept constant for the "living" compartments, at values proposed by Takahashi et al. (1985). The internal Fe contents of both phytoplankton groups

Biogeosciences Discuss., doi:10.5194/bg-2016-153, 2016
Manuscript under review for journal Biogeosciences
Published: 30 May 2016

and Si contents of diatoms are prognostically simulated as a function of ambient concentrations in nutrients and light level. Details on the red-green-blue model by which light penetration profiles are calculated, are given in Lengaigne et al. (2007). The Chl/C ratio is modelled using a modified version of the photo-adaptation model by Geider et al. (1998). For a more detailed description, manuals for NEMO and PISCES are available online at http: //www.nemo-ocean.eu/About-NEMO/Reference-manuals.

The regional configuration used in this study is an Indian Ocean sub-domain of the global ¼° resolution (i.e. cell size ~25 km) configuration described by Barnier et al. (2006). It has 46 vertical levels, with a resolution ranging from 5 m at the surface to 250 m at the bottom. The African continent closes the western boundary of the domain. The oceanic portions of the eastern, northern and southern boundaries use radiative open boundaries (Treguier et al., 2001), constrained with a 150-day relaxation timescale to outputs from a global simulation (Dussin et al., 2009). The circulation and thermodynamics of this regional configuration have been extensively evaluated and reproduce observed intraseasonal variations of key physical parameters well in several Indian Ocean regions (Akhil et al. 2014; Praveen Kumar et al. 2014), including the Arabian Sea (Nisha et al., 2013; Vialard et al., 2013; Keerthi et al., 2015).

The simulation starts from rest, with temperature and salinity initialized from the WOA13. PISCES biogeochemical tracers are also initialized from the WOA13 database for nutrient and from the climatology of a global simulation for the other tracers (Aumont and Bopp 2006). After 5 years of spin-up with a climatological forcing, the model is forced with the Drakkar Forcing Set #4.4 (DFS4.4, Brodeau et al., 2010) from 1980 to 2012. This forcing is a modified version of the CORE dataset (Large and Yeager, 2004), with atmospheric parameters derived from ERA40 reanalysis (Uppala et al., 2005) and ECMWF analysis after 2002 for latent and sensible heat fluxes computation. Radiative fluxes are taken from the corrected International Satellite Cloud Climatology Project-Flux Dataset (ISCCP-FD) surface radiations (Zhang et al., 2004) while precipitation forcing are a blend of satellite products described in Large and Yeager (2004). All atmospheric fields are corrected to avoid temporal discontinuities and to remove known biases (see Brodeau et al. 2010 for details). In the following, we will analyse the 1993-2012 period.

3 Evaluation of the interannual variability in the Northern Arabian Sea

In this section, we provide an intercomparison of the six ocean colour products described above (Section 3.1) and a brief description on model performance at seasonal and interannual time scales in our targeted region (Section 3.2).

3.1 Satellite SChl products intercomparison

One of the major limitations of ocean colour imagery is the inability to perform accurate retrievals under clouds and in presence of aerosols. In the AS, this is particularly challenging during the summer monsoon but not during winter when the

Biogeosciences Discuss., doi:10.5194/bg-2016-153, 2016
Manuscript under review for journal Biogeosciences
Published: 30 May 2016

data coverage is larger than 85% for all datasets considered, and reaches 98% in the case of the merged products (Table 1). Figure 3a shows the SChl climatological seasonal cycle averaged over the NAS region for the six available satellite products. This figure reveals a good agreement between the different products in terms of seasonal phasing, with a semi-annual cycle associated with two seasonal blooms, one in summer (maximum in July, except for MERIS) and the other in winter (maximum in February for all products). The amplitudes of these seasonal blooms however clearly differ depending on the product, with largest blooms in MODIS (up to 2 $mg.m^{-3}$ in winter and 5 $mg.m^{-3}$ in summer) while seasonal blooms hardly reach 1 $mg.m^{-3}$ in GSM.

Large interannual deviations from this climatological evolution occur in all products, as illustrated on Fig. 3b in the case of the OC-CCI product. The largest interannual variability occurs in July, when the monthly standard deviation reaches nearly half of the mean climatological value. A significant although weaker interannual variability is also evident during the winter bloom, with largest deviations occurring during February and March (Fig. 3b). In the following, we define winter as the period encompassing these large climatological and interannual SChl signals, i.e. from January to April. The amplitude of the winter bloom interannual variations however considerably varies amongst SChl products, as illustrated on Fig. 3c. MODIS displays the largest winter standard deviation (~0.4 $mg.m^{-3}$) and OC-CCI and MERIS the weakest ones (~0.1$mg.m^{-3}$). This indicates that the analysis of interannual SChl fluctuations may heavily depend on the product considered.

Scatterplots of monthly SChl interannual anomalies from the different products are shown on Fig. 4. Despite varying amplitudes amongst products, there is generally a good phase agreement between the monthly anomalies from the different products, with correlation ranging from 0.55 between AVW and MODIS to 0.96 between OC-CCI and MERIS. Amongst the three merged products, OC-CCI displays the best match with the three individual satellite products, with a correlation of 0.84, 0.96 and 0.92 with MODIS, MERIS and SeaWiFS, respectively. As already suggested by Fig. 3c, the amplitude of the anomalies from the merged products generally matches the one of MERIS (with regression coefficients ranging from 0.85 to 1.37) but are considerably lower than the ones estimated by MODIS (regression coefficients ranging between 0.23 and 0.43). In the following, most results will be illustrated with the OC-CCI product that displays the best phase agreement with the three individual satellite products (Fig. 3), offers a very good coverage (Table 1) and spans the longest period (1997-2013). It must however be kept in mind that the amplitude of the interannual SChl anomalies remains uncertain, given the large discrepancies amongst products. In the following, we however show that the interannual relationships existing between SChl and ocean physical parameters are generally robust amongst ocean color products.

3.2 Model evaluation

A brief evaluation of the seasonal cycle of SChl in the model simulation follows. The model accurately captures the large-scale surface SChl patterns in the AS for both summer (Fig. 5a, c) and winter (Fig. 5b, d). As for observations, the largest SChl bloom occurs in summer along the Oman coast while the winter bloom is maximum in the northernmost part of the AS

Biogeosciences Discuss., doi:10.5194/bg-2016-153, 2016
Manuscript under review for journal Biogeosciences
Published: 30 May 2016

(Fig. 5b, d). The modelled seasonal SChl evolution agrees well with the OC-CCI data in terms of amplitude and timing (Fig. 6a, d), with a clear semi-annual cycle characterized by a larger SChl bloom during summer (up to 1.5 $mg.m^{-3}$) than in winter (up to 1 $mg.m^{-3}$) and minimum SChl concentrations (less than 0.5 $mg.m^{-3}$) during inter-monsoons. The winter bloom in the NAS occurs in response to convective vertical mixing and related MLD deepening (Fig. 6a, b) driven by the cold, dry northeasterly winds (McCreary and Kundu, 1989; Madhupratab et al., 1996; Prasanna Kumar et al., 2001; Wiggert et al., 2000; Lévy et al., 2007; Kone et al., 2009). The model captures the main features of subsurface physical and biogeochemical variations (Fig. 6b, e): the winter bloom is triggered by the deepening of the mixed layer associated with a strong cooling by surface heat fluxes (Fig. 6c, f), accompanied by a deepening of the thermocline and nitracline. The maximum MLD deepening occurs in January in the model and observations (Fig. 6b, e), one month before SChl peak (Fig. 6a, d). From then on, the upper ocean restratifies and the MLD shoals in response to increased net heat fluxes into the ocean (Fig. 6c, f). This MLD shoaling combined with a nitracline that remains deep (Fig. 6b) limits further nitrate supply to the MLD. This analysis briefly illustrates the ability of the model to capture the main biogeochemical features and related mechanisms in the NAS in winter.

This simulation not only properly captures the SChl seasonal cycle in the NAS region but also its winter interannual variability. Figure 1 provides a first illustration of the model's ability to capture the amplitude of the contrasted surface blooms during the 2007 and 2008 winters discussed in the introduction. Consistent with the observations, the simulation displays a winter bloom that extends further south in 2008 than in 2007, resulting in larger mean SChl concentrations over the NAS region in 2008. Figure 7a provides a more thorough validation of the model interannual SChl variations in this region. Observed winter SChl interannual anomalies range from +0.4 $mg.m^{-3}$ (winter 2012) to -0.3 $mg.m^{-3}$ (winter 2013; Fig. 7a). The largest observed winter positive anomalies are found during 2012, 2008, 2003, 2001 and 2000 (Fig. 7a), while the strongest negative anomalies are found in 1998, 2004, 2007, 2009, 2011 and 2013 (Fig. 7a). The modelled NAS winter interannual SChl anomalies agree generally well with those from the OC-CCI dataset both in terms of phase and amplitude (Fig. 7a), with a correlation between the two time series reaching 0.73 over the 2002-2012 period and 0.53 over the 1998-2012 period, both significant at the 99% confidence level. The main mismatch is found during 1998 and 2003 when the model and observational datasets display opposite anomalies. The observed MLD also exhibits large fluctuations, ranging from -23m in winter 2007 to around ~+14m in winter 2002, 2008 and 2012 (Fig. 7b). The model is also able to capture these observed MLD interannual variations (Fig. 7b), with a 0.68 correlation over the 2002-2012 period significant at the 95% confidence level. The main disagreement between the model and observations occur during the winters of 2003 and 2009, where the observed signals are not well captured by the model. Finally, the observed TCD also exhibits large year-to-year variations in winter, ranging from -15m in winter 2008 and 2010 to ~+15m in winter 2002. In contrast to SChl and MLD, the model does not capture the observed TCD variability well (0.3 correlation), although some major events such as the thermocline shoaling in 2008 and 2010 and the deepening in 2012 are properly simulated. However, the good agreement between the modelled and observed interannual SChl variability in NAS allows us to confidently use the model over a longer

Biogeosciences Discuss., doi:10.5194/bg-2016-153, 2016
Manuscript under review for journal Biogeosciences
Published: 30 May 2016

period (1993-2012) to further investigate interannual chlorophyll variability and its driving mechanisms.

4 Physical drivers of the interannual SChl variability

In this section, we describe how the main characteristics of the interannual chlorophyll variations in the NAS relate to ocean physical properties (MLD, TCD). The hypotheses of Wiggert et al. (2002) and Prasanna Kumar et al. (2001) for the mechanisms that controls SChl interannual variations imply a correlation of SChl anomalies with TCD and MLD anomalies, respectively. In order to test those hypotheses, we compared the time evolution of the OC-CCI SChl, MLD and TCD anomalies in the NAS box from 2002 to 2013 in Fig. 8. This figure illustrates that observed interannual SChl anomalies are closely related to interannual MLD fluctuations, with deeper MLDs generally associated with a positive chlorophyll anomaly, and vice-versa. This is verified for most winters, except 2003 and 2005, where positive chlorophyll anomalies are concomitant with a modest shoaling. In addition, there is a consistent time lag between the MLD and SChl anomalies, with MLD anomalies usually peaking in February and chlorophyll anomalies peaking one month later. In contrast, there is no obvious connection between TCD and SChl anomalies (Fig. 8b): positive SChl anomalies can be either associated with thermocline deepening such as in 2012 or a thermocline shoaling as in 2003 and 2008. Similarly, negative SChl anomalies can be associated to a thermocline deepening as in 2007 or to a shoaling as in 2009 and 2013.

A more quantitative examination of the relationship between interannual SChl anomalies and MLD/TCD anomalies is provided in Fig. 9. As shown in Fig. 9a,c, the winter-averaged SChl and MLD anomalies are strongly correlated in both observations (0.67, statistically significant at the 99% confidence level; Fig. 9a) and the model (0.6 correlation significant at the 99% confidence level; Fig. 9c). In contrast, there is no statistically significant correlation at the 90% confidence level between SChl and TCD variations over the same period for the two datasets (Fig. 9b,d). The dependency of these relationships to the ocean color product used is shown in Table 2. This table indicates that all observational products display larger correlations between SChl and MLD than between SChl and TCD anomalies. The strength of the MLD/SChl relationship however varies depending on the product considered, with the largest correlation for MODIS (0.87) and the weakest for the AVW product (0.40, not significant at the 90% significance level). None of the SChl products exhibits a significant relationship with TCD at the 90% confidence level (Table 2). These results are a strong indication that interannual SChl variations are controlled by MLD rather than by TCD variability.

The spatial distribution of the typical SChl, MLD and TCD anomalies during an anomalously strong bloom event is shown in Fig. 10 for both observations and model. This composite pattern is constructed from the half-difference between positive and negative events highlighted on Fig. 7 for model and Fig. 8 for observations. Observations and model exhibit very similar spatial patterns: the maximum SChl anomaly signal (exceeding 0.5 $mg.m^{-3}$) occupies the northern part of the box around 21°N, 64°E (Fig. 10a,e), with weaker but still significant SChl signals found everywhere in the NAS box. This SChl pattern

Biogeosciences Discuss., doi:10.5194/bg-2016-153, 2016
Manuscript under review for journal Biogeosciences
Published: 30 May 2016

matches well with the MLD pattern, with maximum MLD positive anomalies (exceeding 16 m) occurring at the northern boundary of the NAS box (Fig. 10b,f and significant positive MLD anomalies everywhere in the NAS box. In contrast, the TCD composite hardly shows any significant anomaly within the NAS box during an anomalous strong bloom (Fig. 10c, g).

The availability of chlorophyll and nitrate data at depth from the model allows going a step further in the description of the processes driving the chlorophyll variability. Figure 11 shows the chlorophyll and nitrate evolution between 100 m and the surface, averaged over the NAS box for the two contrasted winters of 2007 and 2008, already discussed on Fig. 1. Both years exhibit a chlorophyll bloom in winter, with maximum chlorophyll concentration in the surface layers in February. The absence of a winter deep chlorophyll maximum (DCM) precludes the entrainment of chlorophyll from below to be responsible for the SChl bloom during this season. This is clearly visible from Fig. 11a,b, which shows that the increase in chlorophyll at the surface layer is not associated with a vertical redistribution of chlorophyll, but with an increase in the vertically integrated biomass.

Let us now investigate what caused this larger phytoplankton growth in winter 2008. The MLD is deepest in January and reaches ~ 50 m during both winters. The similar maximum winter MLDs induce a similar amount of nutrients entrained into the mixed layer (nitrate concentration of 7.23 $mmol.m^{-3}$ in January 2007 against 7.29 $mmol.m^{-3}$ in January 2008) and similar SChl concentrations in January. The main difference between the two winter blooms is their duration: the 2007 bloom ends in mid-February, while the 2008 bloom persists until March (Fig. 11). In terms of the MLD, one of the main differences is that it remained deep until February in 2008 (~50m), but started shoaling one month earlier in 2007. The deeper MLD in February in 2008 is associated with sustained nutrients fluxes toward the surface. As a result, the mixed layer nitrate concentration reaches ~8 $mmol.m^{-3}$ in February 2008 against ~4 $mmol.m^{-3}$ in 2007, hence sustaining more SChl growth in 2008. It must also be noticed that differences in nitracline depths cannot explain the bloom differences between these two winters: it is indeed slightly deeper in 2008 than in 2007 (red lines on Fig. 11).

Figure 12 allows exploring if the processes observed for the 2007 and 2008 contrasted winters also operate to explain SChl winter anomalies over the entire period. As the largest winter MLD and SChl variability occurs in February-March (see Fig. 7 and 8) the analysis in Fig. 12 is restricted to the February-March period. Figure 12a shows that the 0-200 m integrated Chl anomalies exhibit an even stronger relationship with MLD fluctuations (0.84 correlation) than with SChl (Fig. 9c; 0.6 correlation), demonstrating that SChl variability does not arise from a vertical redistribution of chlorophyll within the water column, but mainly results from phytoplankton growth. In addition, larger MLD interannual anomalies are associated with more nutrients in the mixed layer over the 20-year period analysed (Fig. 12b), with a 0.63 correlation between the two parameters. This can occur either through a modulation of the maximum MLD and hence of the amount of nutrients entrained into the mixed layer, or through the period when the MLD is deep (as for 2007/2008) and hence through turbulent fluxes of nutrients into the MLD. As the interannual nitrate anomalies averaged over the mixed layer are correlated with both

Biogeosciences Discuss., doi:10.5194/bg-2016-153, 2016
Manuscript under review for journal Biogeosciences
Published: 30 May 2016

the MLD interannual anomalies (Fig. 12b, 0.63 correlation) and the maximum absolute MLD (not shown; 0.60 correlation), it however not possible to discriminate between the two processes. In any case, the above results suggest that interannual winter chlorophyll variations largely result from phytoplankton growth through nutrient input to the MLD through turbulent processes. Although these results are consistent with Prasanna Kumar et al. (2001) hypothesis, it does not preclude Marra and Barber (2005) hypothesis to operate, i.e. a MLD control through a modulation of the grazing pressure.

Figure 12 also allows discussing the processes driving the interannual MLD variability in winter. There is a significant relationship between the modelled interannual MLD and net surface heat fluxes (Fig. 12c, -0.83 correlation) anomalies during winter. The typical spatial pattern of anomalous net heat flux displays a broad heat flux cooling over the entire northern AS, with maximum anomalies located at the northern end of the AS for both model and observation (Fig. 10d, h). This is consistent with a MLD deepening controlled by convective overturning, which in turn is controlled by surface heat fluxes. Interannual net heat flux variations in this region are strongly related to 2-m air temperature anomalies (Fig. 12d, correlation 0.63), indicative of southward advection of anomalously cold/warm air from the continent driving anomalous blooms, as already suggested by Keerthi et al. (2015). A significant relationship also exists between the modelled interannual MLD variability and sea surface temperature (SST) variability in winter (Fig. 12e). A deeper MLD is associated with a cooler SST (-0.69 correlation), which in turn is driven by net heat flux variability (Fig. 12f, 0.66 correlation). This finally results in a large -0.79 negative correlation between the SST and SChl winter interannual anomalies, because they are both initially driven by the same surface heat flux anomalies. Observations exhibit a similar correlation (-0.73), reinforcing the above conclusions from the model results.

5 Summary and discussion

5.1 Summary

The AS is one of the most productive regions in the world ocean, with a strong monsoon-driven seasonal cycle in SChl. The largest SChl bloom occurs during the summer monsoon in the western AS, in response to coastal and offshore upwelling driven by the Findlater jet. There is however also a prominent SChl bloom in winter in the northern AS, which exhibits large year-to-year fluctuations in its extent and intensity. These variations have not yet been described in detail and there is no consensus on their driving mechanism. In this paper, we described the NAS winter bloom interannual variability and the mechanism driving this variability. To reach that goal, we combined the analysis of several observational datasets (remotely sensed chlorophyll products from various satellites and physical oceanic parameters derived from Argo in-situ profiles) and a biogeochemical model simulation.

Biogeosciences Discuss., doi:10.5194/bg-2016-153, 2016
Manuscript under review for journal Biogeosciences
Published: 30 May 2016

Our results reveal that SChl anomalies from the various satellite products exhibit a good phase agreement, but large amplitude discrepancies. There is a strong (~ +/- 50% of the climatological value) year-to-year variability of the NAS winter SChl bloom. These fluctuations of the bloom amplitude are much better correlated (r~0.4 to 0.87 depending on the satellite product) to MLD than to TCD (r~-0.2 to -0.06) interannual fluctuations. As a result, correlations with MLD interannual anomalies are significant at the 90% confidence level in four out of six chlorophyll satellite products, but are insignificant for TCD anomalies irrespective of the product.

The above analysis is based on a limited number of years in observations, due to the in-situ data temporal coverage, which only becomes sufficient after 2002 thanks to Argo profilers. Using a biogeochemical model allows us extending our analyses over a longer period (1993-2012) and to analyse subsurface chlorophyll data (which are not available from observations). The model agrees well with observations in terms of both MLD and SChl winter interannual anomalies averaged over the NAS (typically r~0.7). Our model however does not include a proper representation of the diurnal cycle, a key ingredient in Wiggert et al. (2002) mechanism that suggests a control of daily dilution through TCD anomalies. In addition, we find no relationship between the winter NAS SChl anomalies and the TCD anomalies in both the model and observations, contrary to what would be expected in Wiggert et al. (2002) mechanism. Rather, we find a strong relationship (r~0.6) between MLD and surface chlorophyll anomalies, as in the observations (r~0.7). The analysis of the model vertical structure indicates that the increase in SChl is not the result of the upward mixing of a pre-existing subsurface chlorophyll maximum. Rather, enhanced surface heat losses due to the advection of cold air by northerly winds result in a more convective overturning, an anomalously deep seasonal MLD and more turbulent fluxes of nutrients into the MLD. This promotes new production in the surface layer. Our study therefore demonstrates that the mechanisms controlling chlorophyll variations at seasonal timescales (Prasanna Kumar et al., 2001; Lévy et al., 2007, Koné et al., 2009) also operate at the interannual timescale.

5.2 Discussion

Our results do not support the hypothesis proposed by Wiggert et al. (2002), i.e. that the TCD in winter controls the bloom amplitude through a daily dilution effect. In contrast, it is consistent with the hypothesis that interannual MLD variations largely control the amplitude of the bloom (Prasanna Kumar et al., 2001; Marra and Barber, 2005). It should be noted that the conclusions from these previous studies relies on the analysis of a very limited number of winters. In addition, the conclusion of Prasanna Kumar et al., (2001) relies on the comparison of MLD in-situ measurements in February 1995 and February 1997, while Wiggert et al. (2002) conclusions largely rely on TCD estimated from an ocean model output. With this in mind, Wiggert et al. (2005) argued that the inconsistency between Prasanna Kumar et al. (2001) and Wiggert et al. (2002) was due to the different seasonal window considered in the two studies: December-January for Wiggert et al. (2002) and February for Prasanna Kumar et al. (2001). Wiggert et al. (2005) argued that during these two periods, phytoplankton growth is driven by two distinct processes. On one hand, the transition from the winter monsoon to the spring inter-monsoon is characterized by detrainment blooms stimulated by increased irradiance received by phytoplankton due to mixed layer

Biogeosciences Discuss., doi:10.5194/bg-2016-153, 2016
Manuscript under review for journal Biogeosciences
Published: 30 May 2016

shoaling that follows the relaxation of monsoon winds. On the other hand, the beginning of the northeast monsoon is characterized by entrainment blooms that are stimulated by the increased in nutrients resulting from a deepening of the mixed layer in that period. To revisit this argument, we repeated our analysis over these two periods (Table 3). Our analysis indicates that interannual SChl anomalies during the beginning of the monsoon period do not exhibit any significant relationship neither with MLD nor with TCD anomalies (correlation below 0.30 not significant at the 90% significance level), i.e. neither Wiggert et al. (2002) mechanism nor Prasanna Kumar et al. (2001) mechanism works during the bloom initiation period. However, a significant relationship exists between SChl anomalies and MLD anomalies during post winter period (February-March) with a correlation of 0.70 in the observations and 0.52 for models (Table 3), suggesting that interannual MLD variations control the amplitude of the bloom during the period of peak interannual variability in winter (February-March).

Our results point towards a strong control of the MLD variability in the NAS by anomalous heat flux. Although we generally refer to interannual MLD variability in this study, the largest MLD fluctuations in NAS are observed over a single month (see Fig. 7b). These variations hence rather occur at intraseasonal timescales but translate into interannual anomalies when averaging over the entire winter season. Keerthi et al. (2015) already provided a detailed description of these intraseasonal MLD fluctuations in this region in winter, relating them to the advection of continental temperature anomalies from the northern end of the basin. The climate variability behind these heat flux fluctuations is however currently unknown. A rapid analysis reveals that interannual variations of the 2-m air temperature in winter in the NAS box is partly correlated with El Nino-Southern Oscillation (ENSO) index (correlation=0.5) and weakly correlated with Indian Ocean Dipole (IOD) index (correlation=0.17), suggesting that part of the winter chlorophyll variations in the NAS are driven by ENSO. However, the exact nature and processes have yet to be understood.

Our model has shown its ability to capture the observed impact of MLD interannual variations on the bloom amplitude in winter in the NAS. However, comparison with another model suggests that this relationship is highly sensitive to the mean state of the model. A rapid examination of the SChl-MLD relationship at interannual timescales in a ½°-global simulation (Bourgeois et al., 2016) forced with the same atmospheric field as our regional model simulation is given on Fig. 13. The correlation between winter interannual SChl and MLD anomalies in this global simulation is of opposite sign (-0.36 correlation, not significant at 90%) to that of our regional model run (Fig. 13g, h, i). This sensitivity cannot be attributed to the version of the biogeochemical model nor to the atmospheric forcing used, because they are virtually the same between these two simulations. In fact, we believe that these differences ensue from differences in mean state simulated in the two models, the mean winter MLD in the global simulation being 30-m deeper than in the observations, while our regional model shows a far better agreement (Fig. 13 d-f). This mean state difference results in a weaker winter surface bloom in the global simulation than in our regional simulation and in observations (Fig. 13 a, c), likely because of light limitation. Variations in light limitation rather than in the amount of nutrient injected in the MLD hence dominates the impact of interannual MLD

variations on the amplitude of the chlorophyll bloom in this global simulation, resulting in an opposite phase relation between SChl and MLD in this simulation compared to observations and to a more realistic simulation.

An obvious perspective of this study is to investigate the processes controlling the interannual chlorophyll variations in summer, which are far larger than in winter. As compared to the winter season, an analysis based on observations during the summer monsoon is complicated by the poorer satellite data coverage (Table 1) and the fewer Argo profiles in the Oman/Somalia upwelling region (Fig. 2b). The model analysis may however provide further insights on the mechanisms that control the upwelling productivity during summer. Long-term variations also deserve further analysis. Goes et al. (2005) suggest that the southwest monsoon intensifies as a result of climate change, driving increased upwelling, primary production and ecosystem changes in the AS. Climate change models however show a large range of responses in terms of changes in the southwest monsoon (e.g. Turner and Annamalai, 2012), and of productivity in the AS (e.g. Bopp et al. 2013). Those large uncertainties call for more targeted studies of the impact of climate change on oceanic productivity in the AS.

Acknowledgments

Keerthi M. G is supported by a Fellowship from CEFIPRA. Model experiments were performed at HPC Pravah at CSIR-NIO. M. Lengaigne, C. Ethé, J. Vialard, M. Levy, de Boyer Montegut and O. Aumont are funded by Institut de Recherche pour le Développement (IRD). Parvathi V is funded by CSIR under SRF. I. Suresh acknowledge the financial support from CSIR, New Delhi. We thank Goddard GSFC/NASA for providing the SeaWiFs, MERIS and MODIS chlorophyll data, ESA-GLOBCOLOUR for providing the GSM and AVW chlorophyll data and ESA-OCEANCOLOUR for providing the OC-CCI chlorophyll data. The NIO contribution number is XXX.

References

Akhil, V. P., Durand, F., Lengaigne, M., Vialard, J., Keerthi, M. G., Gopalakrishna, V. V., Deltel, C., Papa, F., de Boyer Montégut, C.: A modelling study of the processes of surface salinity seasonal cycle in the Bay of Bengal, J. Geophys. Res., 116, 3926-3947, doi: 10.1002/2013JC009632, 2014

Aumont, O. and Bopp, L.: Globalizing results from ocean in-situ iron fertilization studies, Global Biogeochem. Cy., 20, GB2017, doi:10.1029/2005GB002591, 2006.

Aumont, O., Ethé, C., Tagliabue, A., Bopp, L., Gehlen, M.: PISCES-v2: an ocean biogeochemical model for carbon and ecosystem studies, Geosci. Model Dev., 8, 2465-2513, doi:10.5194/gmd-8-2465-2015, 2015.

Banse, K. and English .D. C. : Revision of satellite-based phytoplankton pigment data from the Arabian Sea during the northeast monsoon, Mar. Res. Pakistan, 2, 83–103, 1993.

Banse, K.and English .D. C. : Geographical differences in seasonality of CZCS-derived phytoplankton pigment in the Arabian Sea for 1978– 1986, Deep Sea Res., Part II, 47, 1623–1677,200.

Banse, K. and McClain, C. R. : Winter blooms of phytoplankton in the Arabian Sea as observed by Coastal Zone Color Scanner, Mar. Ecol. Prog. Ser., 34, 201– 211, 1986.

Banzon, V. F., Evans, R.E., Gordon, H.R., Chomko, R.M. : SeaWiFS observations of the Arabian Sea southwest monsoon bloom for the year 2000, Deep Sea Res., Part II, 51, 189– 208, 2004.

Barber, R.T., Marra, J., Bidigare, R.C., Codispoti, L.A., Halpern, D., Johnson, Z., Latasa, M., Goericke, R., Smith, S.L. : Primary productivity and its regulation in the Arabian Sea during 1995. Deep-Sea Research II 48, 1127–1172, 2001.

Barnier, B., Madec, G., Penduff, T., Molines, J., Treguier, A., Sommer, J. L., Beckmann, A., Biastoch, A., Boning, C., Dengg, J.,Derval, C., Durand, E., Gulev, S., Remy, E., Talandier, C., Theetten, S., Maltrud, M., McClean, J., and Cuevas, B. D.: Impact of partial steps and momentum advection schemes in a global ocean circulation model at eddy permitting resolution, Ocean Dynam.,56, 543–567, doi:10.1007/s10236-006-0082-1, 2006.

Bauer, S., Hitchcock, G. L., and Olson, D. B.: Influence of monsoonally-forced Ekman dynamics upon the surface-layer depth and plankton biomass distribution in the Arabian Sea, Deep-Sea Res., 38, 531–553, 1991.

Bopp, L., Resplandy, L., Orr, J.C., Doney, S.C., Dunne, J.P., Gehlen, M., Halloran, P., Heinze, C., Ilyina, T., Seferian, R. and Tjiputra, J. : Multiple stressors of ocean ecosystems in the 21st century: projections with CMIP5 models, 2013.

Bourgeois, T., Orr, J. C., Resplandy, L., Ethé, C., Gehlen, M., and Bopp, L.: Coastal-ocean uptake of anthropogenic carbon, Biogeosciences Discuss., doi:10.5194/bg-2016-57, in review, 2016

Boyer, T. P., Antonov, J. I., Baranova, O. K., Coleman, C., Garcia, H. E., Grodsky, A., Johnson, D. R., Locarnini, R. A., Mishonov, A. V., O'Brien, T. D., Paver, C. R., Reagan, J. R., Seidov, D., Smolyar, I. V., and Zweng, M. M.: World Ocean Database 2013, NOAA Atlas NESDIS 72, S. Levitus, Ed., A. Mishonov, Technical Ed.; Silver Spring, MD, 209 pp., 2013

Brodeau, L., Barnier, B., Treguier, A.M., Penduff, T., Gulev, S. : An ERA 40-based atmospheric forcing for global ocean circulation models. Sci Direct 31:88–104. doi:10.1016/j.ocemod.2009.10.005, 2010

Dickey, T., Marra, J., Sigurdson, D.E., Weller, R.A., Kinkade, C.S., Zedler, S.E., Wiggert, J.D., Langdon, C. : Seasonal variability of biooptical and physical properties in the Arabian Sea: October 1994–October 1995. Deep Sea Res Part II 45(10):2001–2025, 1998.

Dussin, R., Treguier A.-M., Molines, J. M., Barnier, B., Penduff, T., Brodeau, L., Madec, G.: Definition of the interannual experiment ORCA025-B83, 1958–2007, LPO Report 902, 2009

Findlater, J.: A major low-level air current near the Indian Ocean during the northern summer, Q. J. R. Meteorol. Soc., 95, 362–380, 1969.

Geider, R. J., MacIntyre, H. L., and Kana, T. M.: A dynamic regulatory model of phytoplanktonic acclimation to light, nutrients, and temperature, Limnol. Oceanogr., 43, 679–694, 1998.

Goes, J. I., Thoppil, P.G., Gomes, H.D., Fasullo, J.T. : Warming of the Eurasian landmass is making the Arabian Sea more productive, Science, 308, 545–547, 2005.

Grant, M., Jackson, T., Chuprin, A., Sathyendranath, S., Zühlke, M., Storm,T., Boettcher, M., Fomferra,N. : Ocean Colour Climate Change Initiative (OC_CCI) – Phase Two, Product User Guide, Plymouth Marine Laboratory, http://www.esa-oceancolour-cci.org/?q=webfm_send/496, 2015.

Gundersen, J.S., Gardner, W.D., Richardson, M.J., Walsh, I.D. : Effects of monsoons on the seasonal and spatial distributions of POC and chlorophyll in the Arabian Sea. Deep-Sea Research II 45, 2103–2132, 1998

Kamykowski, D. and Zentara, S. J. : Hypoxia in the world ocean as recorded in the historical data set, Deep Sea Research Part A. Oceanographic Research Papers, 37(12), 1861-1874, 1990.

Keerthi, M.G., Lengaigne, M., Vialard, J., de Boyer Montegut, C., Muraleedharan, P.M. : Interannual variability of the Tropical Indian Ocean mixed layer depth. Clim Dyn 40:743–759, 2013.

Keerthi M.G., Lengaigne, M., Drushka, K., Vialard, J., de Boyer Montégut, C., Pous, S., Levy, M., and Muraleedharan, P. M.: Intraseasonal variability of mixed layer depth in the tropical Indian, Clim. Dyn., doi:10.1007/s00382-015-2721-z, 2015

Koné, V., Aumont, O., Lévy, M., and Resplandy, L.: Physical and Bio-geochemical controls of the Phytoplankton Seasonal Cycle in the Indian Ocean: a modeling study. in: Wiggert J. D., Hood, R. R., Naqvi, S. W. A., Brink, K. H., and Smith, S. L., 185, 147–166, American Geophysical Union, Washington DC, USA, 2009.

Large, W. G., Yeager, S. G.: Diurnal to decadal global forcing for ocean and sea-ice models: the data sets and flux climatologies. NCAR/TN-460 STR, 111 pp, 2004

Lengaigne, M., Menkes, C., Aumont, O., Gorgues, T., Bopp, L., Andre, J. M., Madec, G.: Influence of the oceanic biology on the tropical Pacific climate in a coupled general circulation model, Climate Dynamics, 28, 503–516, 2007.

Levy, M., Shankar, D., Andre, J. M., Shenoi S. S. C., Durand, F., de Boyer, C., Montegut, C.: Basinwide seasonal evolution of the Indian Ocean's phytoplankton blooms. J Geophys Res 112:C12014, 2007.

Madec, G.: NEMO, the ocean engine, Note du Pole de modelisation, Institut Pierre-Simon Laplace (IPSL), France, No 27 ISSN No 1288–1619, available at: "http://www.nemo-ocean.eu/About-"www.nemo-ocean.eu/About-NEMO/Reference-manuals, 2008.

Madhupratap, M., Kumar, S. P., Bhattathiri, P. M. A., Kumar, M. D., Raghukumar, S., Nair, K. K. C., and Ramaiah, N.: Mechanism of the biological response to winter cooling in the northeastern Arabian Sea, Nature, 384, 549–552, 1996

Maritorena, S. and Siegel, D.A. : Consistent Merging of Satellite Ocean Colour Data Sets Using a Bio-Optical Model. Remote Sensing of Environment , 94, 4, 429-440, 2005.

Marra, J. and Barber, D. : Primary production in the Arabian Sea: A synthesis of JGOFS data, Prog. Oceanogr., 65, 159–175, 2005.

McCreary, J.P., Murtugudde, R., Vialard, J., Vinayachandran, P.N., Wiggert, J.D., Hood, R.R., Shankar, D. and Shetye, S. : Biophysical processes in the Indian Ocean. Indian Ocean Biogeochemical Processes and Ecological Variability, pp.9-32, 2009.

McCreary, J.P. and Kundu, P. K. : A numerical investigation of sea surface temperature variability in the Arabian Sea. J Geophys Res 94:16097–16114, 1989.

Nisha, K., Lengaigne, M., Gopalakrishna, V. V., Vialard, J., Pous, S., Peter, A-C., Durand, F., Naik, S.: Processes of summer intraseasonal sea surface temperature variability along the coasts of India, Ocean Dynamics, 63, 329-346, 2013.

O'Reilly, J. E., Maritorena, S., Siegel, D. A., O'Brien, M. C., Tool, D., Mitchell, B. G., Karhu, M., Chavez, F. P., Strutton, P., Cota, G., Hooker, S. B., McClain, C. R., Carder, K. L., Muller-Karger, F., Harding, L., Magnusson, A., Phinney, D., Moore, G. F., Aiken, J., Arrigo, K. R., Letelier, R., Culver, M. : Ocean color chlorophyll-a algorithms for SeaWiFS, OC2 and OC4: Version 4. In S. B. Hooker, & E. R. Firestone (Eds.), SeaWiFS postlaunch technical report series 11 SeaWiFS postlaunch calibration and validation analyses: Part 3 (pp. 9–23). Greenbelt, MD: NASA Goddard Space Flight Center, 2000.

Prasanna Kumar, S., Madhupratap, M., Dileep Kumar, M., Gauns, M., Muraleedharan, P.M., Sarma, V.V.S., De Souza, S.N. : Physical control of primary productivity on a seasonal scale in central and eastern Arabian Sea, Deep Sea Res.: 433-441, 2000.

Prasanna Kumar, S.., Ramaiah, N., Gauns, M., Sarma, V., Muraleedharan, P.M., Raghukumar, S., Kumar, M.D., Madhupratap, M. : Physical forcing of biological productivity in the northern Arabian Sea during the Northeast Monsoon, Deep-Sea Research II 48, 1115–1126, 2001.

Praveen Kumar, B., Vialard, J., Lengaigne, M., Murty, V.S.N., McPhaden, M.J. : TropFlux: Air-Sea Fluxes for the Global Tropical Oceans – Description and evaluation. Climate Dynamics 38:1521- 1543. Doi:10.1007/s00382-011-1115-0, 2012.

Praveen Kumar B., Vialard, J., Lengaigne, M., Murty, V. S. N., Foltz, G., McPhaden, M. J., Pous, S., and de Boyer Montégut, C.: Processes of interannual mixed layer temperature variability in the Thermocline Ridge of the Indian Ocean, Clim. Dyn., 43, 2377-2397, 2014.

Resplandy, L., Levy, M., Madec, G., Pous, S., Aumont, O., and Kumar, D.: Contribution of mesoscale processes to nutrient budgets in the Arabian Sea, J. Geophys. Res., 116, C11007, doi: 10.1029/2011JC007006, 2011.

Sarma, V. V. S. S.: The influence of Indian Ocean Dipole (IOD) on biogeochemistry of carbon in the Arabian Sea during 1997—1998, J. Earth Syst. Sci., 115(4), 433–450, doi:10.1007/BF02702872, 2006.

Sarma, Y. V. B., Adnan Al Azri., Smith, L.S . : Inter-annual Variability of Chlorophyll-a in the Arabian Sea and its Gulfs, International Journal of Marine Science 2.1, 2012.

Satya Prakash and Ramesh, R. : Is the Arabian Sea getting more productive?. Current Science, 92(5), 667-670, 2007.

Schott, F. and McCreary, J. P. : The monsoon circulation of the Indian Ocean, Prog. Oceanogr., 51, 1– 123, 2001.

Smith, S.L. and Madhupratap, M. : Mesozooplankton of the Arabian Sea: patterns influenced by seasons, upwelling, and oxygen concentrations. Progress in Oceanography, this issue, doi:10.1016/j.pocean.2005.03.007, 2005.

Smith, S. L., Roman, M., Prusova, I., Wishner, K., Gowing, M., Codispoti, L. A., et al. : Seasonal response of zooplankton to monsoonal reversals in the Arabian Sea. Deep-Sea Research II, 45, 2369–2403, 1998.

Takahashi, T., Broecker, W. S., and Langer, S.: Redfield ratio based on chemical data from isopycnal surfaces, J. Geophys. Res., 90,6907–6924, 1985.

Treguier, A., Barnier, B., de Miranda, A., Molines, J. M., Grima, N., Imbard, M., Madec, G., Messager, C., Reynaud, T., and Michel, S.: An eddy-permitting model of the Atlantic circulation: Evaluating open boundary conditions, J. Geophys. Res., 106, 22115– 22129, 2001.

Turner, A. G. and Annamalai, H.: Climate Change and the South Asian Monsoon, *Nature Climate Change* **2**: 587-595, doi: 10.1038/nclimate1495, 2012.

Uppala, S.M. et al. : The ERA-40 re-analysis. Q J R Meteorol Soc 131:2961–3012, 2005.

Vialard, J., Drushka, K., Bellenger, H., Lengaigne, M., Pous, S., Duvel, J-P.: Understanding Madden–Julian-induced sea surface temperature variations in the North Western Australian Basin. Clim Dyn. Doi: 10.1007/s00382-012-1541-7, 2013.

Wiggert, J. D., Hood, R., Banse, K., and Kindle, J.: Monsoon driven biogeochemical processes in the Arabian Sea, Progr. Oceanogr., 65, 176–213, doi:10.1016/j.pocean.2005.03.008, theArabian Sea of the 1990s: New Biogeochemical Understanding, 2005.

Wiggert, J. D., Jones, B. H., Dickey, T. D., Brink, K.H., Weller, R. A., Marra, J., Codispoti , L. A. : The northeast monsoon's impact on mixing, phytoplankton biomass and nutrient cycling in the Arabian Sea, Deep Sea Res., Part II, 47, 1353– 1385, 2000.

Wiggert, J. D., Murtugudde, R., and McClain, C. R.: Processes controlling interannual variations in wintertime (northeast monsoon) primary productivity in the central Arabian Sea, Deep Sea Res., Part II, 47,2319 – 2343, 2002.

Zhang, Y. C., Rossow, W. B., Lacis, A. A., Oinas, V., Mishchenko, M. I.: Calculation of radiative fluxes from the surface to top of atmosphere based on ISCCP and other global data sets: refinments of the radiative transfer model and the input data. J Geophys Res 109:D19105. doi: 10.1029/2003JD004457, 2004.

Biogeosciences Discuss., doi:10.5194/bg-2016-153, 2016
Manuscript under review for journal Biogeosciences
Published: 30 May 2016

Tables

Name	Satellite	Algorithm	Period	Grid	Winter/Summer NAS coverage
SeaWiFs	GeoEye OrbView- 2	OC4v6 (O'Reily et al, 2000)	1997- 2010	9km	86%/ 25%
MERIS	ESA ENVISAT	OC4Me (O'Reily et al, 2000)	2002-2012	9km	88%/ 30%
MODIS	Terra and Aqua	ESA ENVISAT OC3v5 (O'Reily et al, 2000	2002-present	9km	90%/ 20%
GSM	Combine SeaWiFs/MODIS/ MERIS	GSM (Maritorena and Siegel, 2005)	1997- 2012	4km	98%/ 45%
AVW	Combine SeaWiFs/MODIS/ MERIS		2002-2012	4km	98%/ 44%
OC-CCI	Combine SeaWiFs/MODIS/ MERIS	OC-CCI-v2.0 (Grant et al 2015)	1997- 2013	4km	98%/ 58%

Table 1: Main characteristics of ocean color satellite products used in the present study

Biogeosciences Discuss., doi:10.5194/bg-2016-153, 2016
Manuscript under review for journal Biogeosciences
Published: 30 May 2016

SChl Data	Cor(MLD)	Cor(TCD)
SeaWiFs (2003-2010)	0.56	-0.16
MERIS (2003-2012)	**0.75**	-0.06
MODIS (2003-2012)	**0.87**	-0.20
OC-CCI (2003-2012)	**0.78**	-0.09
GSM (2003-2012)	**0.80**	-0.20
AVW (2003-2012)	0.40	-0.16

Table 2: Correlation between NAS box-averaged winter (January-April) SChl anomalies derived from satellite products and in-situ MLD and TCD anomalies. Bold typeface indicates correlations, which are statistically different from zero at the 90% confidence level.

5

Biogeosciences Discuss., doi:10.5194/bg-2016-153, 2016
Manuscript under review for journal Biogeosciences
Published: 30 May 2016

		Correlation		
		January-April **(JFMA)**	December-January **(DJ)**	February-March **(FM)**
OC-CCI	**MLD Vs SChl**	**0.67**	0.20	**0.70**
	TCD Vs SChl	-0.12	0.34	-0.09
Model	**MLD Vs SChl**	**0.60**	-0.30	**0.52**
	TCD Vs SChl	0.28	-0.17	0.33

Table 3: Correlation between SChl and MLD and TCD anomalies averaged over the NAS box for January-April, December-January and February-March. Bold typeface indicates correlations, which are statistically different from zero at the 90% confidence level.

Biogeosciences Discuss., doi:10.5194/bg-2016-153, 2016
Manuscript under review for journal Biogeosciences
Published: 30 May 2016

Figures

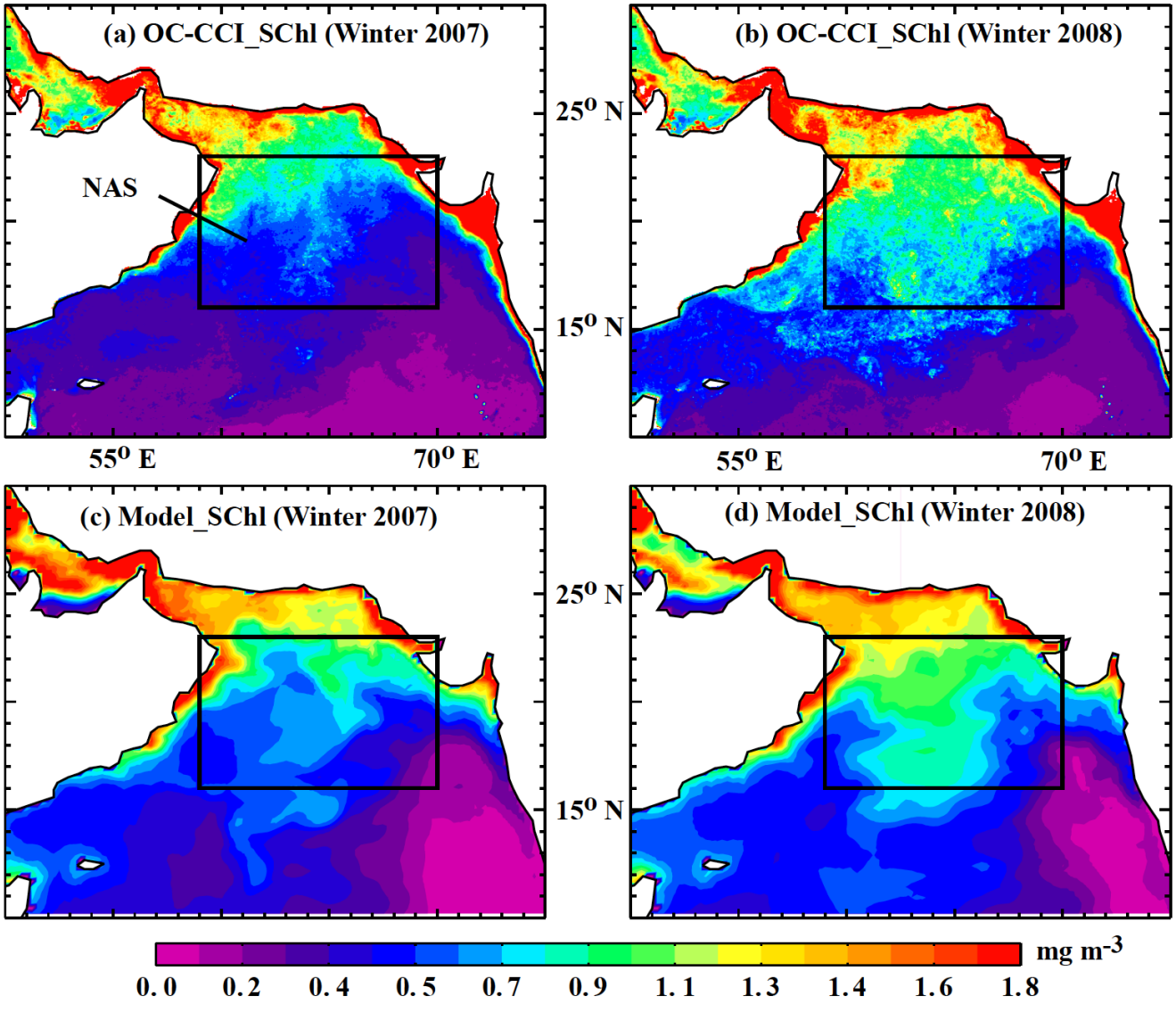

Figure 1: Arabian Sea average SChl for the winter (January-April) of **(left panels)** 2007 and **(right panels)** 2008 in **(top)** OC-CCI product and **(bottom)** model. The NAS (North Arabian Sea) box (59°E-70°E, 16°N-23°N) is indicated by a black frame for future reference.

Biogeosciences Discuss., doi:10.5194/bg-2016-153, 2016
Manuscript under review for journal Biogeosciences
Published: 30 May 2016

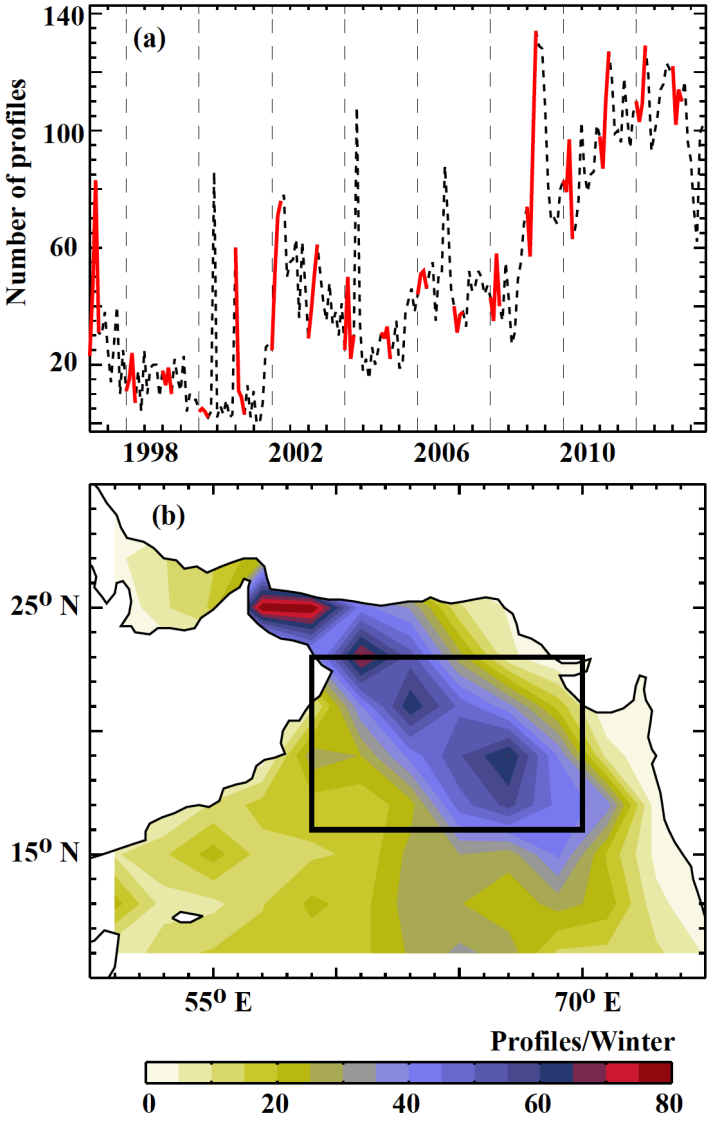

Figure 2: (a) Time series of the number of in-situ profiles per month over the NAS box, from 1997 to 2013. The curve is highlighted in red for winter (January-April). **(b)** Average winter in-situ profiles density (per 2°x2° box and per season) for 2002-2013. The NAS region is indicated by a black frame on panel b.

Biogeosciences Discuss., doi:10.5194/bg-2016-153, 2016
Manuscript under review for journal Biogeosciences
Published: 30 May 2016

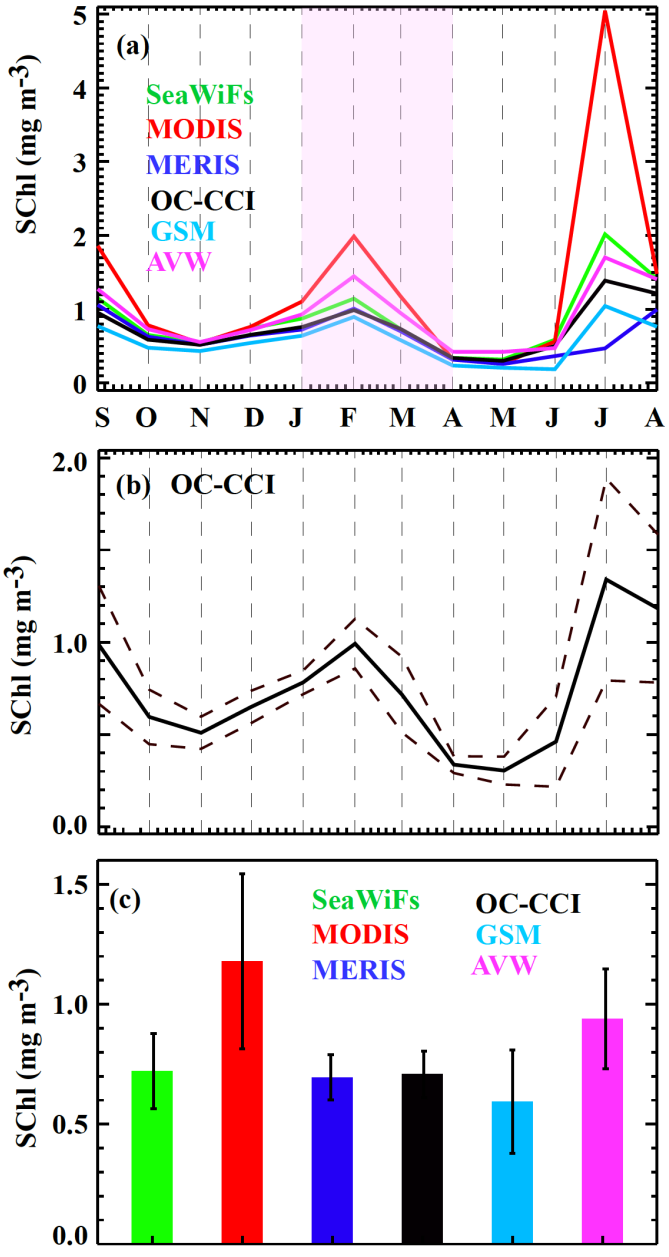

Figure 3. (a) Climatological monthly seasonal cycle of NAS-averaged SChl for all satellite products. **(b)** Climatological monthly seasonal cycle of NAS-averaged OC-CCI SChl (plain black curve) and envelope displaying the interannual variability amplitude (+/- 1 standard deviation, dashed black line). **(c)** Mean (bars) and +/- one standard deviation (whiskers) of winter (JFMA) SChl for each product.

Biogeosciences Discuss., doi:10.5194/bg-2016-153, 2016
Manuscript under review for journal Biogeosciences
Published: 30 May 2016

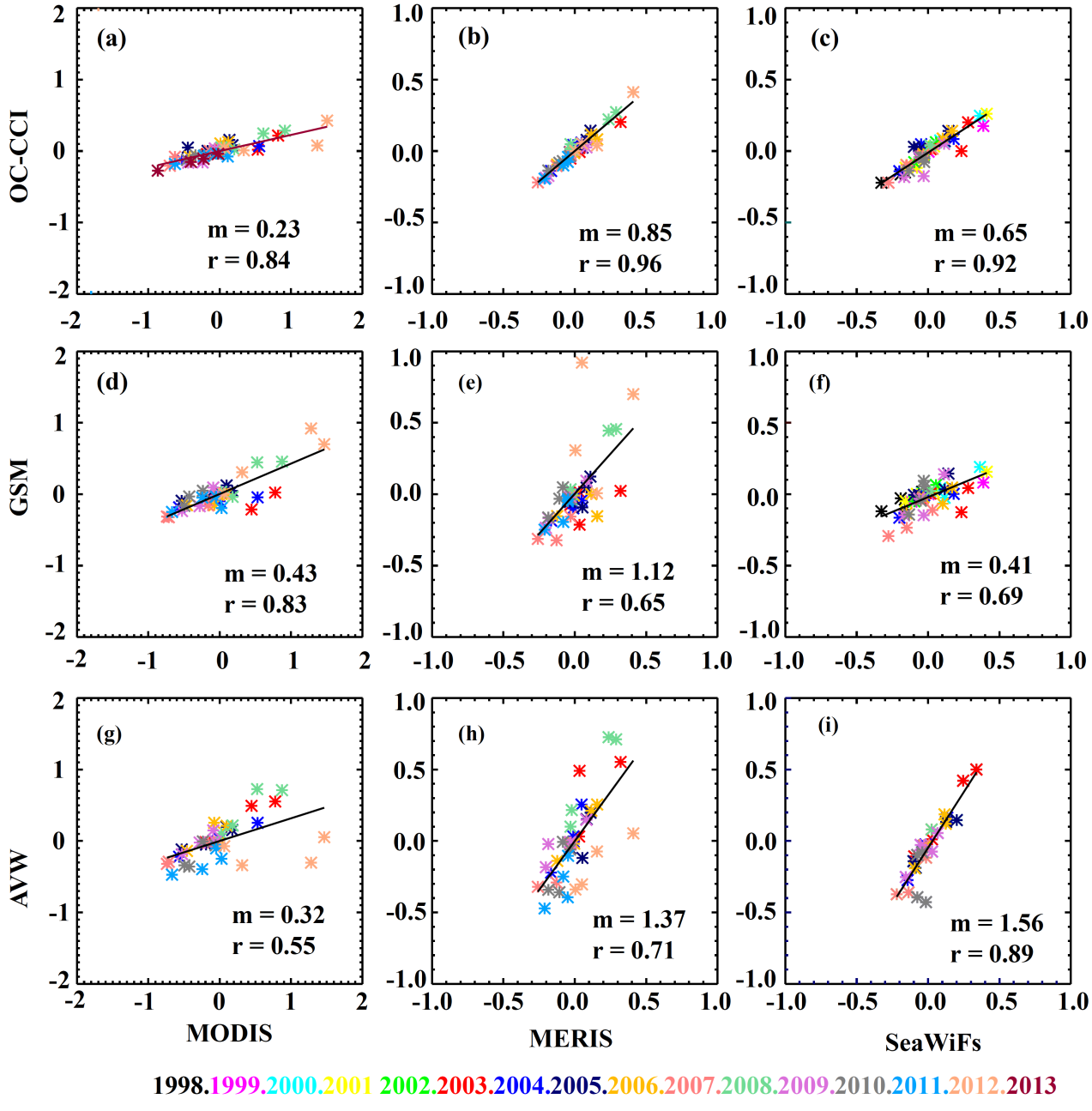

Figure 4. (First row) Scatter plot of NAS-averaged winter (January-April) monthly SChl interannual anomalies (mg.m^{-3}) in OC-CCI product against MODIS, MERIS and SeaWiFs products. **(Second row)** Idem for GSM product. **(Third row)** Idem for AVW product. All the correlations (r) and regression coefficients (m) indicated on each panel are significantly different from zero at the 90% confidence level.

Biogeosciences Discuss., doi:10.5194/bg-2016-153, 2016
Manuscript under review for journal Biogeosciences
Published: 30 May 2016

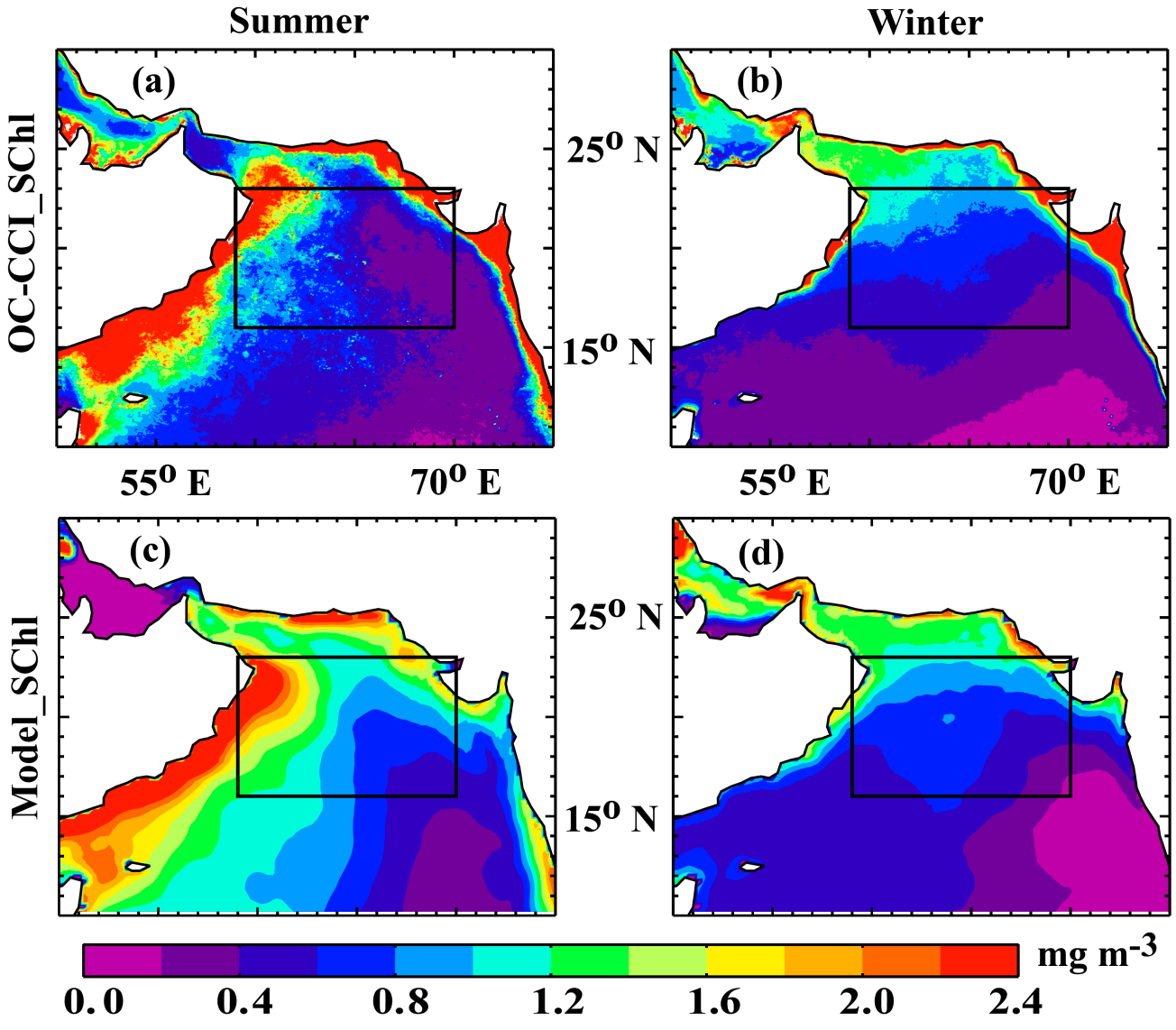

Figure 5: Arabian Sea climatology of (left panels) summer (June-September) and (right panels) winter (January-April) **(top)** OC-CCI and **(bottom)** modeled SChl (mg.m^{-3}).

Biogeosciences Discuss., doi:10.5194/bg-2016-153, 2016
Manuscript under review for journal Biogeosciences
Published: 30 May 2016

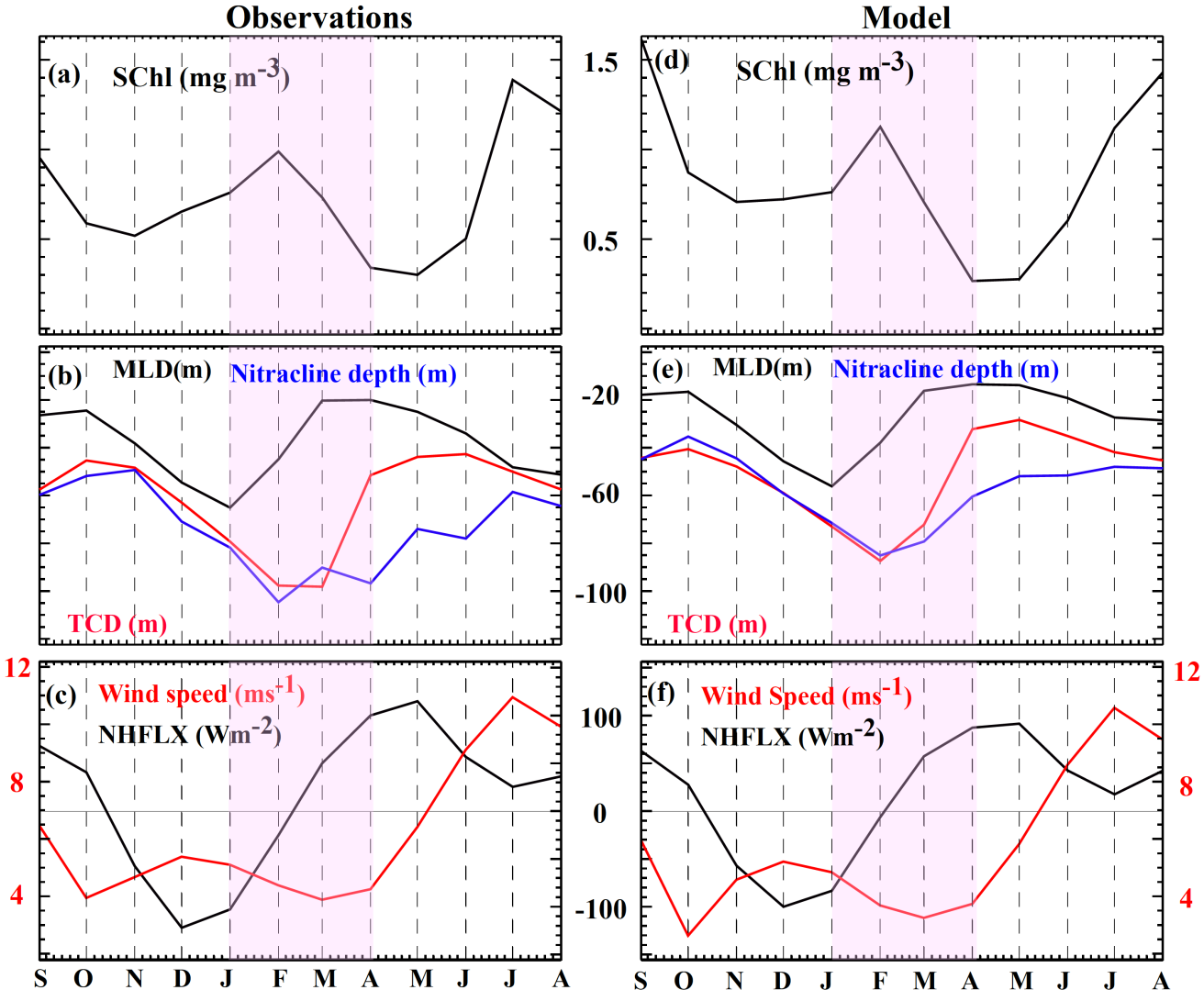

Figure 6: Mean seasonal cycle of NAS box-averaged monthly **(a)** SChl, **(b)** MLD (black line), TCD (red line) and nitracline depth (blue line), **(c)** surface net heat flux (NHFLX) and wind speed in observations. **(d-f)** Same for model. The NAS box is marked on Fig. 1.

Biogeosciences Discuss., doi:10.5194/bg-2016-153, 2016
Manuscript under review for journal Biogeosciences
Published: 30 May 2016

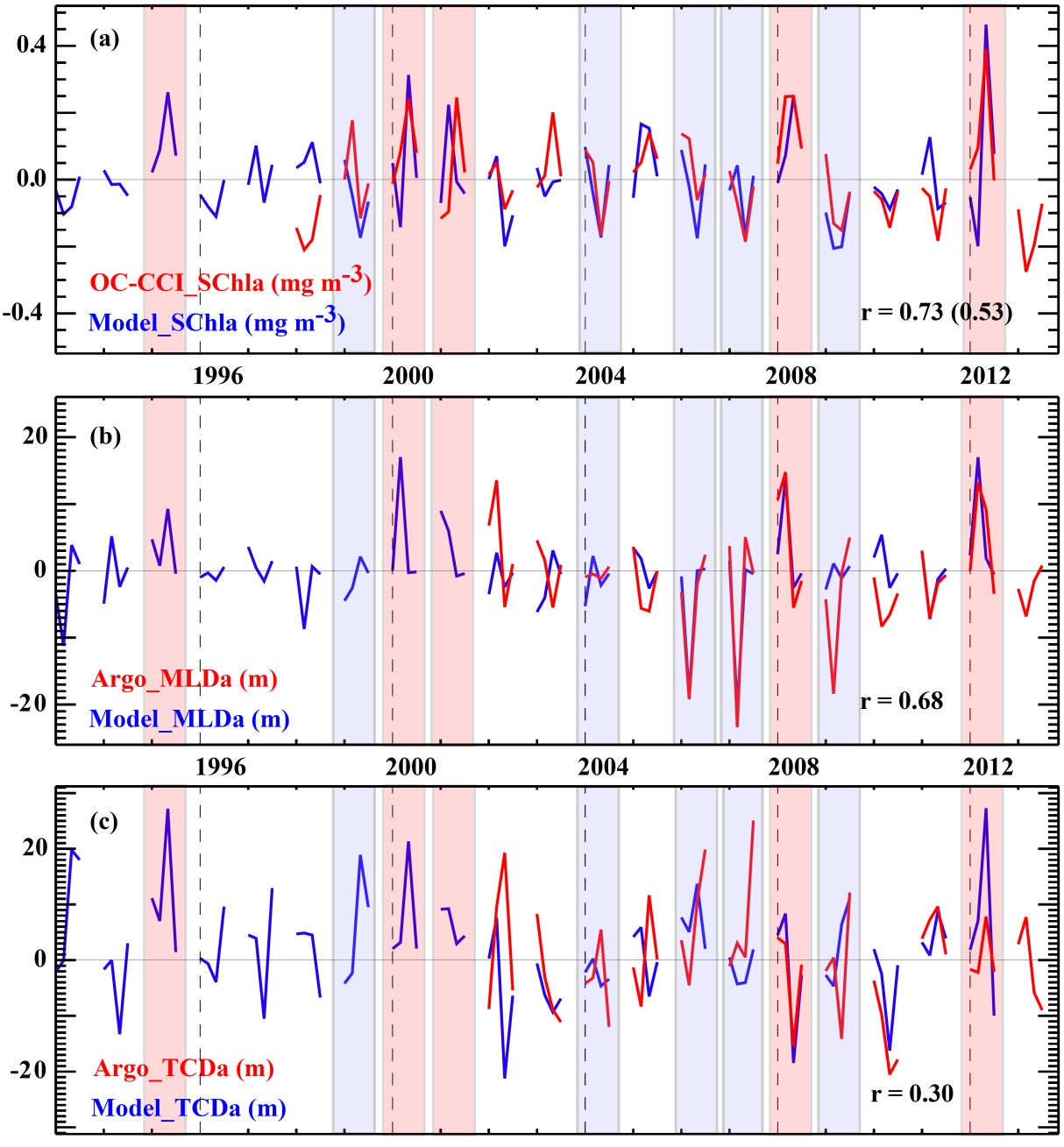

Figure 7: Monthly time series of winter (January-April) NAS box-averaged modeled and observed interannual anomalies of **(a)** SChl, **(b)** MLD and **(c)** TCD. The correlation between the model and observations from 2002-2012 is indicated on panels (a-c). The value in bracket in (a) is the correlation during 1998-2012. Red and blue shadings respectively indicate winters for strong and weak blooms in the model, considered for the composite plots of Fig. 10.

Biogeosciences Discuss., doi:10.5194/bg-2016-153, 2016
Manuscript under review for journal Biogeosciences
Published: 30 May 2016

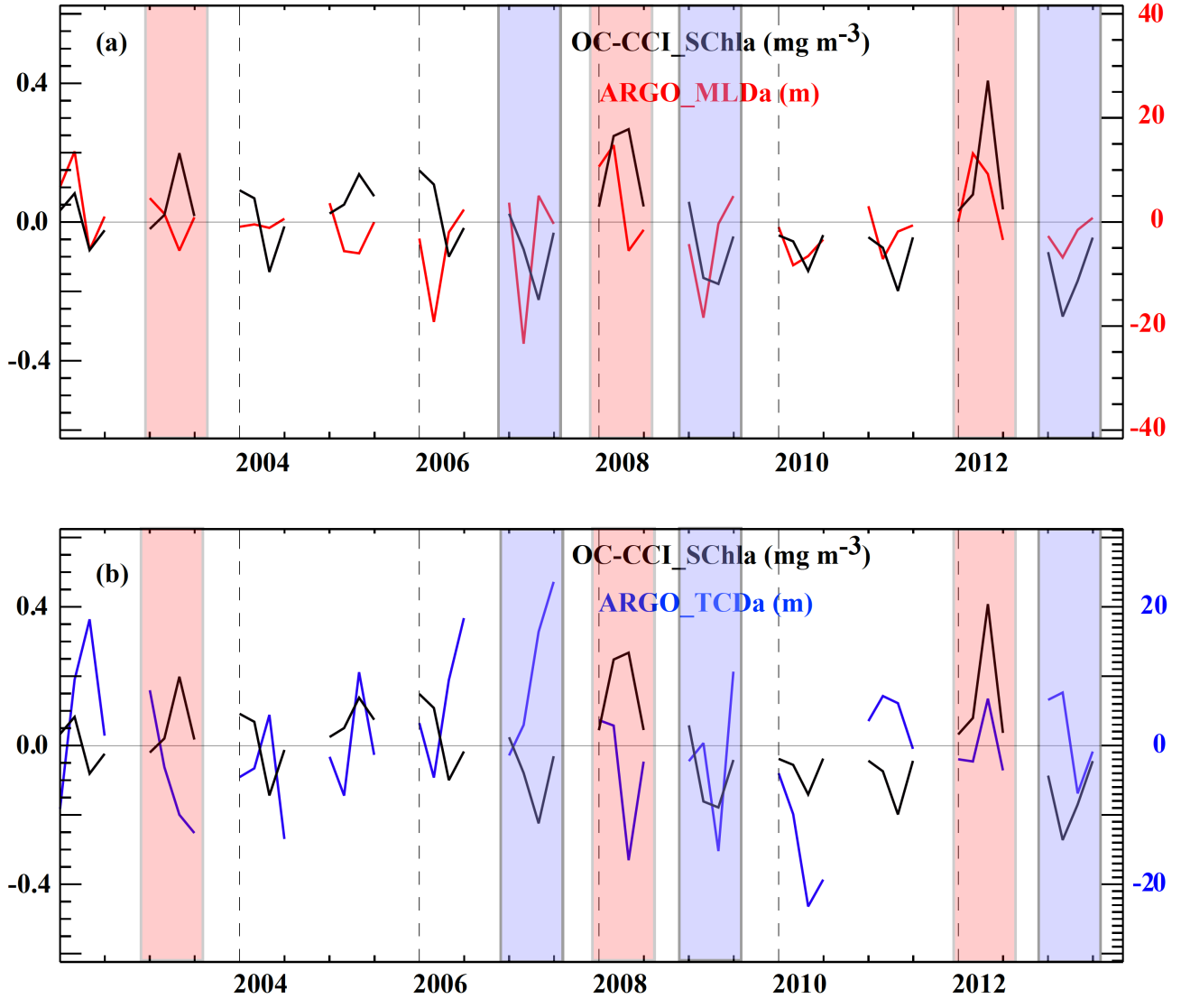

Figure 8: Observed monthly time series of winter (January-April) NAS box-averaged **(a)** SChl and MLD and **(b)** SChl and TCD anomalies over the 2002-2013 period. The red (blue) shadings highlight the winters of strong (weak) blooms used in the composite plots of Fig. 10.

Biogeosciences Discuss., doi:10.5194/bg-2016-153, 2016
Manuscript under review for journal Biogeosciences
Published: 30 May 2016

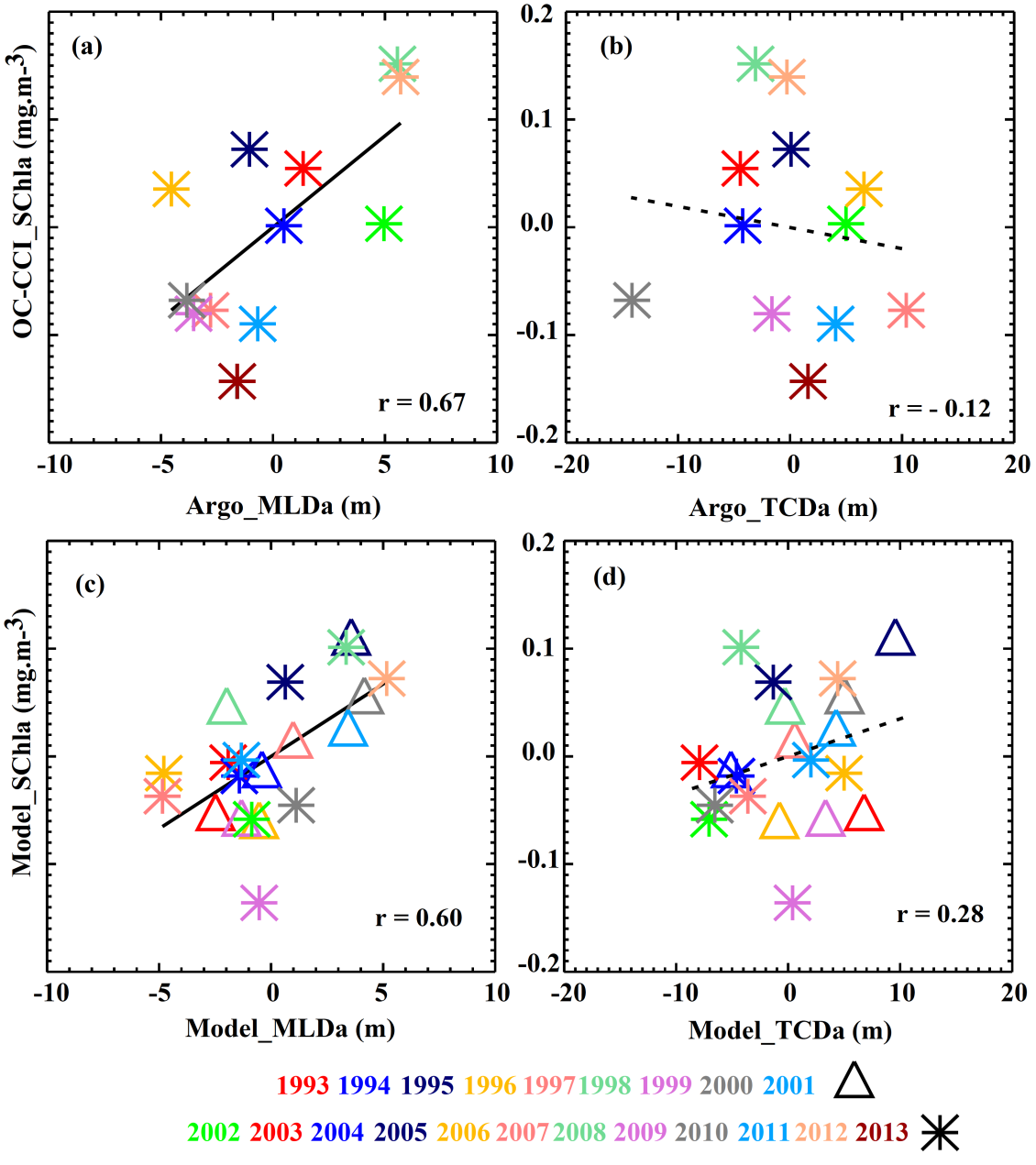

Figure 9: Scatterplot of winter (January-April), NAS-averaged OC-CCI SChl anomalies against observed **(a)** MLD and **(b)** TCD anomalies. **(c-d)** Idem for Model.

Biogeosciences Discuss., doi:10.5194/bg-2016-153, 2016
Manuscript under review for journal Biogeosciences
Published: 30 May 2016

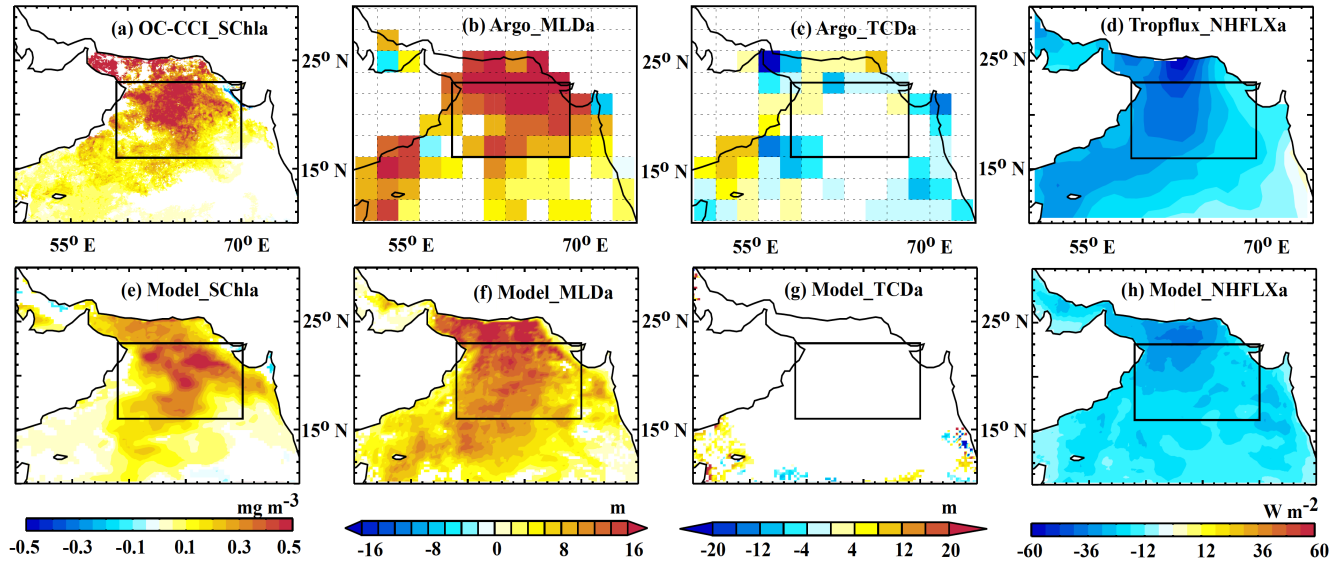

Figure 10: Observed interannual anomalies of **(a)** SChl (OC-CCI), **(b)** MLD and **(c)** TCD (Argo-derived) **(d)** net surface heat flux (Tropflux NHFLX) for composite SChl blooms (built from half of the difference between positive and negative events highlighted on Fig. 8). The SChl composites are built from the months of max SChl anomaly: March 2003, March 2008 and March 2012 for positive events; March 2007, March 2009 and February 2013 for negative events. The MLD and TCD composites are built from the months of February of the same year). **(e-h)** Idem for the model. For the model, composites are built from the positive and negative events highlighted on Fig. 7 (SChl is composited using March 1995, 2000, 2008, 2012 and February 2001 for positive events and March 1999, 2004, 2006, 2007, 2009 for negative events; MLD and TCD are composited using February of the same years). Regions where composite values are less than the standard error are displayed in white.

Biogeosciences Discuss., doi:10.5194/bg-2016-153, 2016
Manuscript under review for journal Biogeosciences
Published: 30 May 2016

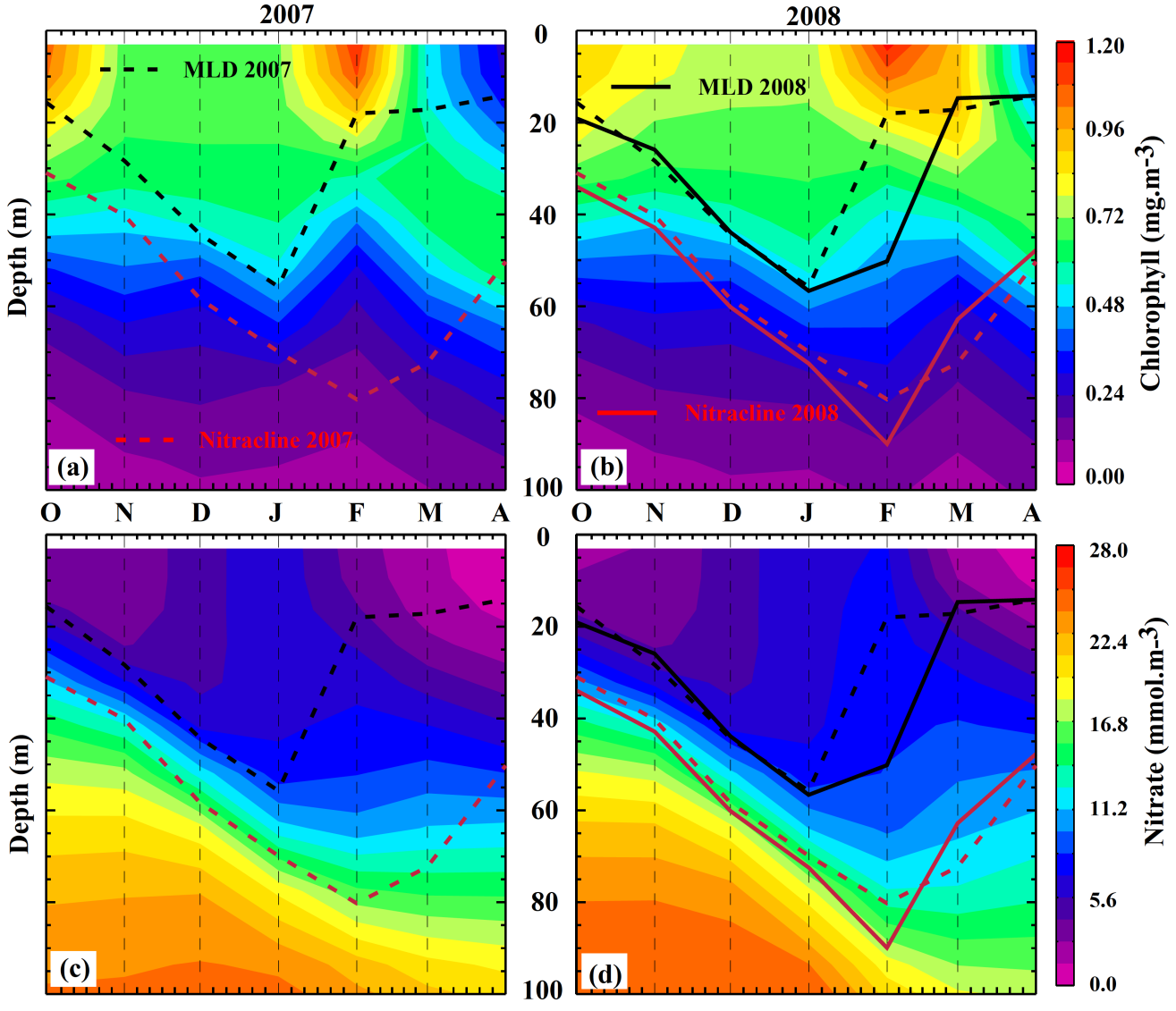

Figure 11: Depth-Time section of NAS-averaged **(a, b)** chlorophyll and **(c, d)** nitrate for **(a, c)** 2007 and **(b, d)** 2008. The black lines indicate the MLD, in thick for 2008 and dashed for 2007. The red lines similarly indicate the nitracline depth.

Biogeosciences Discuss., doi:10.5194/bg-2016-153, 2016
Manuscript under review for journal Biogeosciences
Published: 30 May 2016

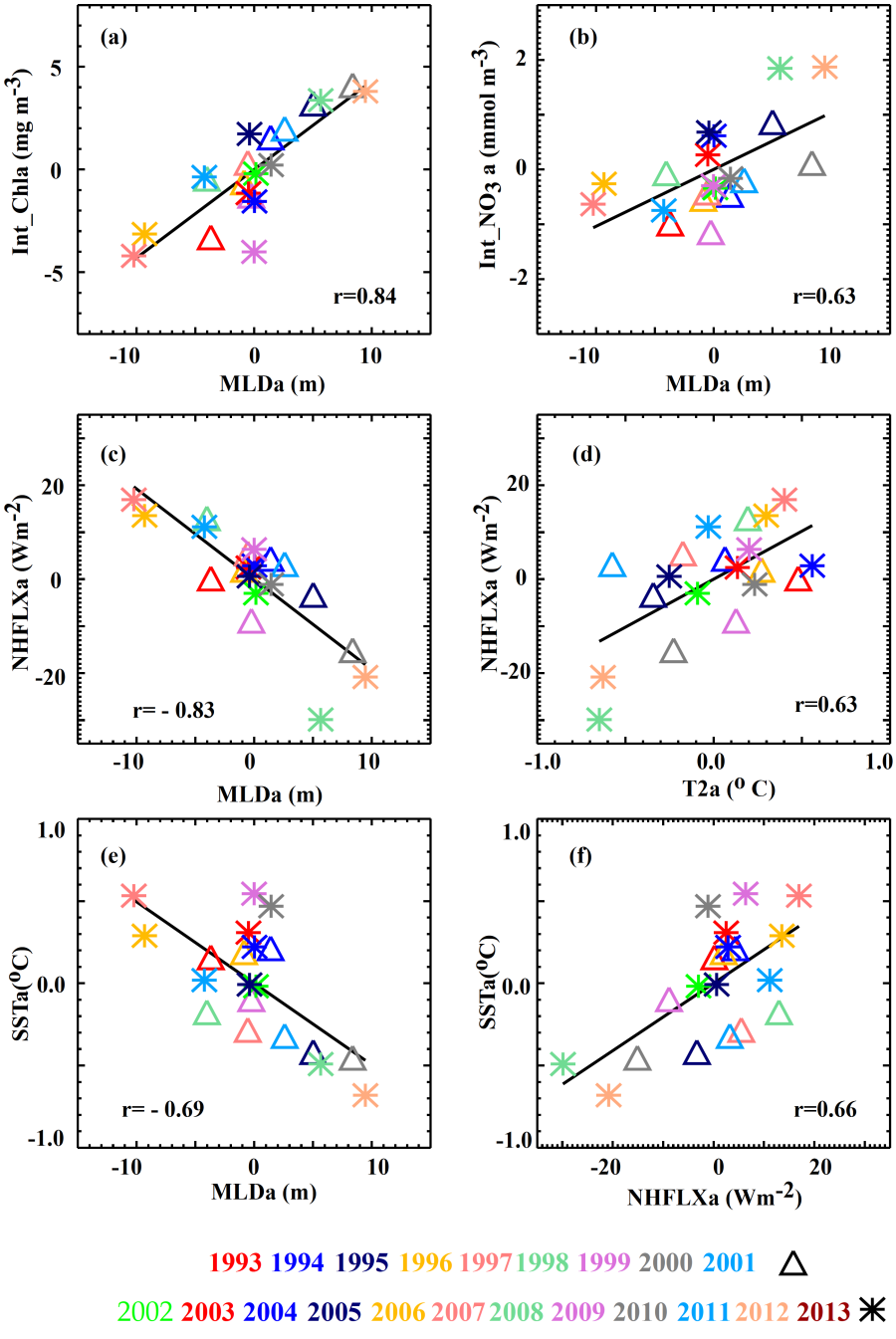

Figure 12: Scatterplot of modeled NAS box-averaged winter (February-March) interannual anomalies of (a) 0-200m total chlorophyll content against MLD. **(b)** Average MLD nitrate vs MLD. **(c)** Surface net heat flux (NHFLX) vs MLD. (d) Surface net heat flux (NHFLX) vs 2-m air temperature (T2). (e) SST vs. MLD. (f) SST vs. surface net heat flux (NHFLX). Plain lines indicate regression coefficients that are significantly different from zero at the 90% confidence level.

Biogeosciences Discuss., doi:10.5194/bg-2016-153, 2016
Manuscript under review for journal Biogeosciences
Published: 30 May 2016

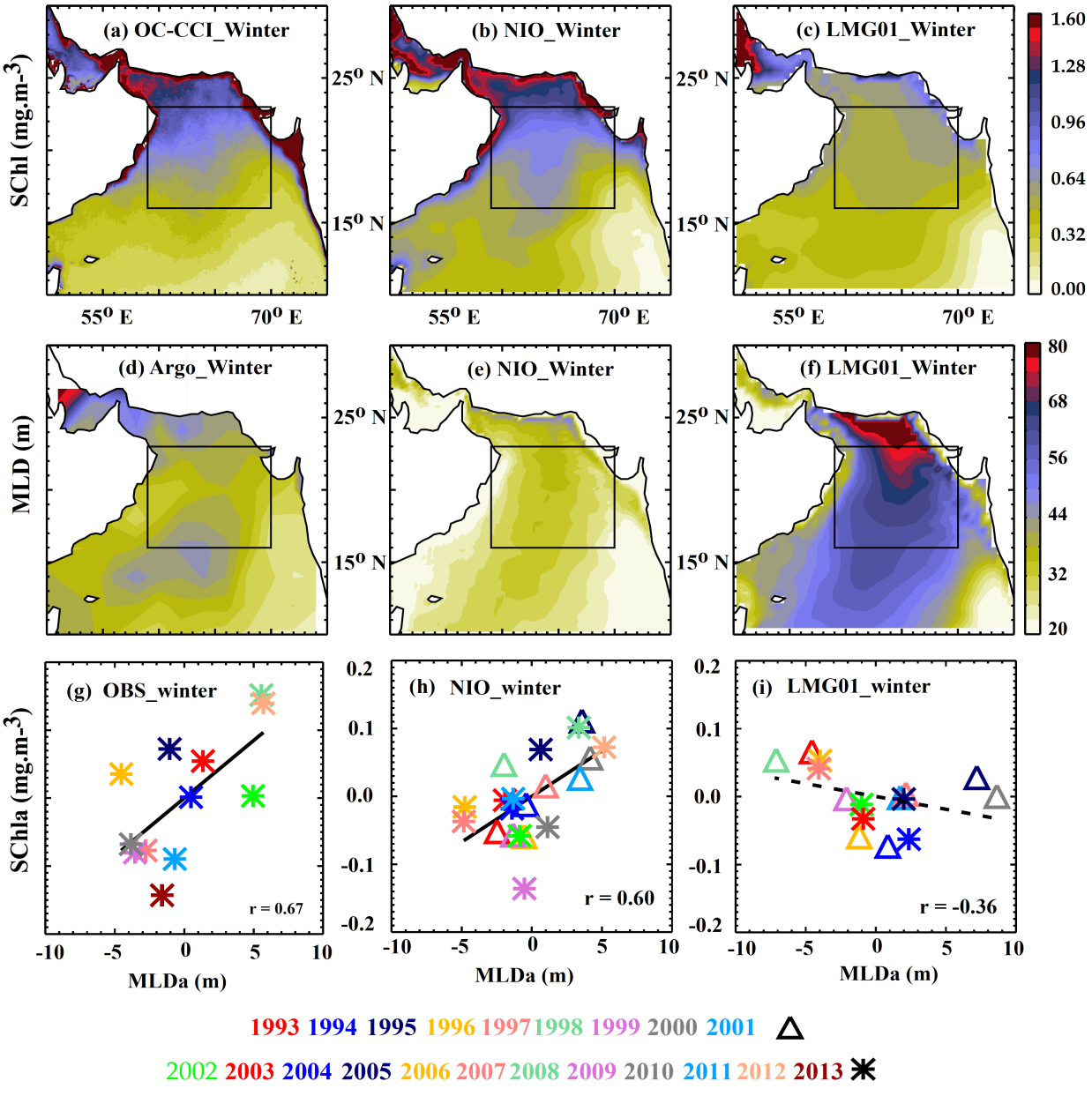

Figure 13: Climatological winter SChl for (a) OC-CCI, (b) Model used in the current study, (c) LMG01 global simulation described in Bourgeois et al. (2016). (d-f) Idem for climatological winter MLD. Scatterplot of NAS box-averaged mean winter SChl anomalies against MLD anomalies for (g) observations (OC-CCI vs in-situ derived estimates), (h) the regional simulation used in the current study and (i) the LMG01 global simulation.